R-00-27

System and safety studies of accelerator driven Transmutation systems

Annual report 1999

Waclaw Gudowski, Jan Wallenius, Marcus Eriksson,
Johan Carlsson, Per Seltborg and Kamil Tucek

Department of Nuclear and Reactor Physics
Royal Institute of Technology, Stockholm

May 2000

Svensk Kärnbränslehantering AB
Swedish Nuclear Fuel
and Waste Management Co
Box 5864
SE-102 40 Stockholm Sweden
Tel 08-459 84 00
+46 8 459 84 00
Fax 08-661 57 19
+46 8 661 57 19

ISSN 1402-3091
SKB Rapport R-00-27

System and safety studies of accelerator driven Transmutation systems

Annual report 1999

Waclaw Gudowski, Jan Wallenius, Marcus Eriksson,
Johan Carlsson, Per Seltborg and Kamil Tucek

Department of Nuclear and Reactor Physics
Royal Institute of Technology, Stockholm

May 2000

PREFACE

In November 1996, SKB commenced funding of the project "System and safety studies of accelerator driven transmutation systems and development of a spallation target". The aim of the project was stated as:

Development of a complete code for simulation of transmutation processes in an accelerator driven system. Application of the code for analysis of neutron flux, transmutation rates, reactivity changes, toxicity and radiation damages in the transmutation core.

Build up of competence regarding issues related to spallation targets, development of research activities regarding relevant material issues. Performing of basic experiments in order to investigate the adequacy of using the spallation target as a neutron source for a transmutation system, and participation in the planning and implementation of an international demonstration experiment.

In the present report, activities within and related to the framework of the project, performed at the department of Nuclear and Reactor Physics at the Royal Institute of Technology during 1999, are accounted for.

SUMMARY IN SWEDISH

SAMMANFATTNING

Inom ramen för SKB-projektet ”System- och säkerhetsstudier” av acceleratordrivna transmutationssystem, samt utveckling av ett spallationstarget har avdelningen för kärn- och reaktorfysik på KTH under år 1999 arbetat med härddesign, utveckling av utbränningskod, reaktordynamikanalys och termohydraulik för underkritiska system. Konstruktionen av spallationstarget har varit under utförande.

Härddesign

Genom att bestråla transuraner i energetiska neutronspektra kan man reducera deras kvardröjande toxicitet med en faktor 100. Underkritiska acceleratordrivna reaktorer kan laddas med bränsle bestående enbart av transuraner utan att säkerhetsmarginaler vid kokning av kylmedel överskrids. Bestrålning av americium i typiska neutronspektra ger dock upphov till problem med bränslesvällning, då α-sönderfall av transmutations-produkten curium ackumulerar heliumgas i bränslestavar. Avdelningen har därför föreslagit en underkritisk härddesign där stavar med anrikad borkarbid spridits ut i bränsleknippen innehållande americium. Isotopen B-10 absorberar då långsamma neutroner och därmed minskar heliumproduktionen i bränslestavarna betydligt. Borkarbidintroduktionen visar sig även möjliggöra minimering av kvot mellan maximum- och minimumeffekt i härden, samt bidra till en minskad reaktivitetsförlust under utbränningen. Nackdelen med förslaget visar sig vara en ökning av reaktiviteten vid kokning av kylmedlet, som dock kan mildras genom att använda bly/vismut som kylmedel istället för natrium.

Utbränningskod och utveckling av tvärsnittsdatabibliotek för neutron/protonenergi upp till 150 MeV

En fullständigt integrerad Monte-Carlo-kod för att beräkna neutronflöden och utbränning i godtyckliga reaktorsystem har utvecklats. Under 1999 har rutiner för hantering av restvärme lagts till koden. Temperaturberoende tvärsnittsbibliotek inkluderande deponering av gammaenergi har producerats. Jämförande studier av kodens förmåga att korrekt beräkna utbränning i förenklade modeller av underkritiska system har utförts, som visat på god överensstämmelse med avancerade deterministiska koder utvecklade i Frankrike. De senare kan dock ej användas för icke-symmetrisk tredimensionell modellering.

Tvärsnittsbibliotek för ^{232}Th, ^{238}U och ^{239}Pu har skapats och genomgår just nu en valideringsprocess för att integreras i generella högenergitvärsnittsbibliotek.

Reaktordynamik

Ett samarbete med Argonne-laboratoriet i USA har lett till att avdelningen kunnat använda en kod anpassad för att beräkna reaktordynamik för underkritiska system. Nya typer av problemscenarier som uppstår i acceleratordrivna reaktorer är bland annat händelseförloppet vid förlust av acceleratorstråle, samt injektion av oönskat hög protonström i spallationstarget. Beräkningar på det förstnämnda fallet visar att temperatur på bränsle och kylmedel sjunker till inloppstemperaturen för kylmedlet efter 10 sekunder.

Termohydraulik

Beräkningar av beteendet hos nödkylsystem avsedda att kunna föra bort restvärme vid fel på kylmedelspumpar har utförts i samarbete med Joint Research Centre-ISPRA. STAR-CD-datakoden har validerats i jämförelse med experimentella resultat från PASCO-loopen i Karlsruhe. Dessutom har simuleringar på två ADS av Ansaldo-design genomförts. Systemen var utformade för 80 respektive 800 MW termisk effekt. Resultaten visar att ett ”Förlust av värmebortföring” (Loss of Heat Sink)-scenario för 80 MWth ADS kan hanteras tillräckligt bra med yttre luftkylning. För ett system med 800 MWth krävs andra åtgärder än enbart yttre luftkylning. För scenariot ”Förlust av värmebortföring” kombinerat med fördröjd avstängning av accelerator kan ett vattensprejsystem mellan reaktor och yttre säkerhetstank väsentligt öka tillgängliga tidsmarginaler, men är ändå inte tillräckligt för permanent kylning.

Simuleringar av MUSE-experimenten

Simuleringar av MASURCA-reaktorn har genomförts för en kritisk och underkritisk konfiguration med en Monte-Carlo simuleringskod. Jämförelse med experiment och andra beräkningar tyder på vissa osäkerheter i tvärsnittsbibliotek som måste förklaras.

Spallationstarget-tillverkning

Samarbete med det institut i Obninsk som tillverkar ett 1 MW Pb/Bi spallationstarget närmar sig den avgörande testfasen. Strålmålet är nu färdigtillverkat och ”off-beam”-tester kommer att genomföras i juni 2000.

TABLE OF CONTENTS

1 INTRODUCTION

The radio-toxic inventory of spent nuclear fuel stays at a level above that of natural uranium for 200 000 years after discharge from a typical light water reactor. The relative contribution to the radio-toxic inventory from the transuranium nuclides are shown in Fig. 1-1. From this figure it can be inferred, that if *both* plutonium and americium are completely transmuted to stable or less long-lived nuclides, the required life-time of a geological repository can be drastically reduced.

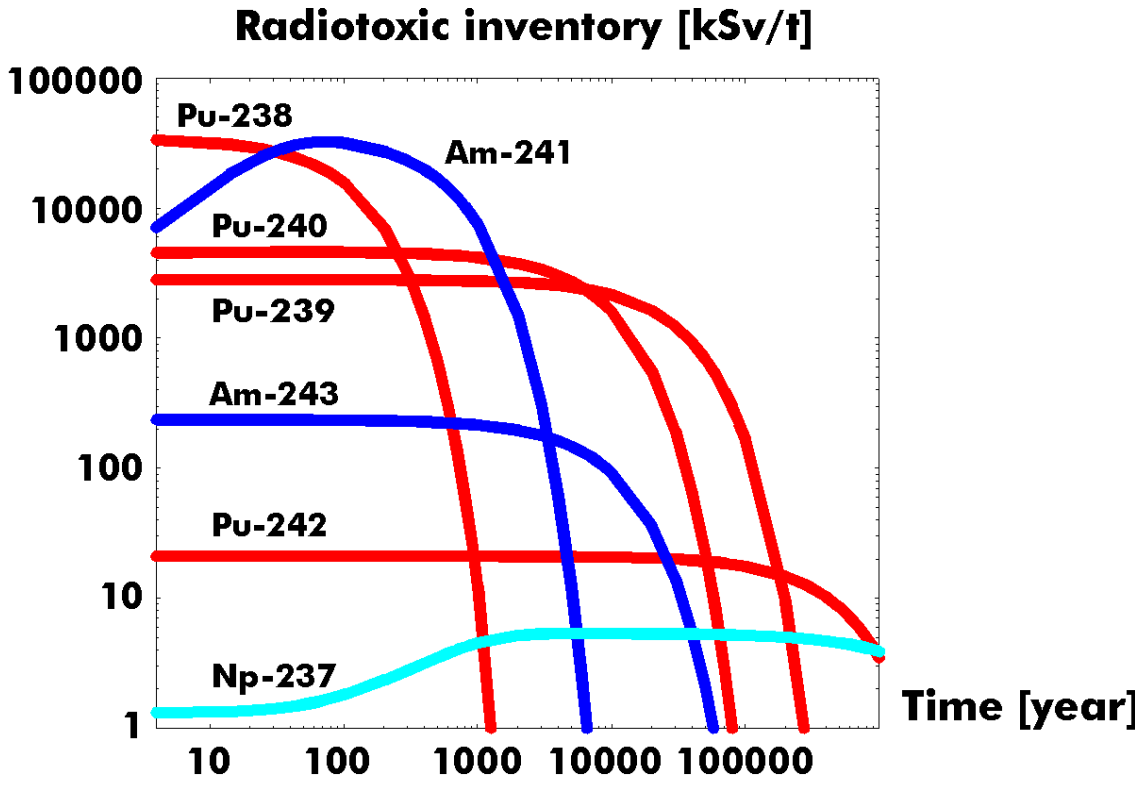

Figure 1-1. Specific radiotoxic inventory of transuranium elements in spent LWR fuel.

It has been shown in a number of papers that existing types critical fast reactors would be able to burn plutonium with a reasonable degree of efficiency [1][2][10]. However, from the safety perspective, a limit in the allowable concentration of minor actinides (i.e. Neptunium, Americium and Curium) in the fissile fuel of about 5% was found. Taken into account the large backlog of americium arising from decay of Pu-241 presently being stored, it was argued that dedicated minor actinide burner reactors must be introduced into any realistic transmutation scenario [1][4].

During the last decade, it has been clarified that due to the lack of Doppler feedback of minor actinide fuels, combined with a very small fraction of delayed neutrons, safety margins for minor actinide burners operating in critical mode would be unacceptably small. Hence, accelerator driven systems (ADS) were identified as an essential part of P&T scenarios in both Japan and France [6][3].

The application of accelerator driven systems for the specific purpose of nuclear waste transmutation was suggested by Los Alamos National Laboratory in the early seventies

[7]. Detailed and realistic design work, was however not made until the Japanese Omega program started in 1988 [8]. Studies of accelerator driven systems at KTH started in 1993. Shortly after this, the CERN proposal of a thorium fuelled ADS attracted a lot of attention in international media [5].

While various concepts of ADS have been suggested, the attention of the detailed design work in Japan, Korea, the United States and Europe is now firmly focused on fast neutron spectrum, solid fuel cores being supplied with source neutrons from a lead-bismuth spallation target. The department of Nuclear and Reactor Physics at KTH is studying in particular a Boron-10 poisoned core that minimises helium production in fuel pins, and hence increases burnup limits (large helium production leads to fuel swelling and eventually fuel pin failure) [11]. In what follows, an account for the work on core design, safety analysis and simulation code development will be given. Further, activities related to spallation target development and sub-critical core physics experiments will be described.

2 CORE DESIGN

The sub-critical system studies at KTH are directed towards a core that would burn not only the comparatively large fraction of americium present in spent Swedish fuel, but also all of the excess plutonium from the existing light water reactor park. Recycling plutonium, as MOX in the LWR:s once may be beneficial for the size of the waste stream to be managed by the accelerator driven systems, as up to 25% of the plutonium inventory could be incinerated to a relatively low cost in this way. In any case, the fraction of plutonium in the transuranium fuel to be directed to the first generation of dedicated transmutation reactors would be in the range of 80 - 85%.

When fabricating and irradiating transuranium fuels in sub-critical systems, a number of problems are expected to arise. For example:

- For fuels with Pu content higher than 50%, reactivity losses when Pu-239 and Pu-241 are burned away are expected to be large. Consequently, power peaking increases with burnup, as does the accelerator power needed to maintain a constant core power.
- The high concentration of fissile nuclides (no U-238 is present) leads to very high power densities in fuel pins.
- Neutron capture in the abundant nuclide Am-241, with subsequent alpha decay of Cm-242 leads to large helium production rates in fuel pins during irradiation. Helium accumulation into bubbles causes fuel pellets to swell, with fuel pin failure as a consequence.
- The appearance of the alpha-emitters Pu-238 and Cm-244 due to neutron capture in Am-241 and Am-243 increases the cost of fuel reprocessing and refabrication, as the (α,n) reaction demands better shielding.

The second of the above issues has previously been addressed by the introduction of diluent materials into the fuel, that would bring down the linear power to acceptable values. Examples of such diluents are $MgAl_2O_4$ (Spinel) for oxide fuels, ZrN for nitride fuels, and Zr for metallic fuels. The drawback of this approach is that the presence of a diluent increases the macroscopic cross section for inelastic scattering, and hence yields significant slowing down of neutrons. In the resulting soft neutron spectrum, the direct fission probability of americium is rather small, about 10%. Consequently problems with production of strong alpha-emitters remain.

An alternative approach that has been explored at KTH is the introduction of burnable absorbers (BA) into the sub-critical core. Such "poisons" would not only alleviate reactivity losses, they would also act as an effective sink for slow neutrons that otherwise may become captured by the minor actinides! Accordingly, we label the poisoned core here investigated as the "Sing Sing Core".

In Figure 2-1, the absorption cross section of boron-10 is shown, in comparison with the capture and fission cross sections of Am-241. It is seen that boron-10 in large concentrations can shield slow neutrons from being captured in Am-241, without deteriorating the probability of fast fission. Enriched boron carbide (92% B-10) thus was selected as the preferred absorber in the present design studies.

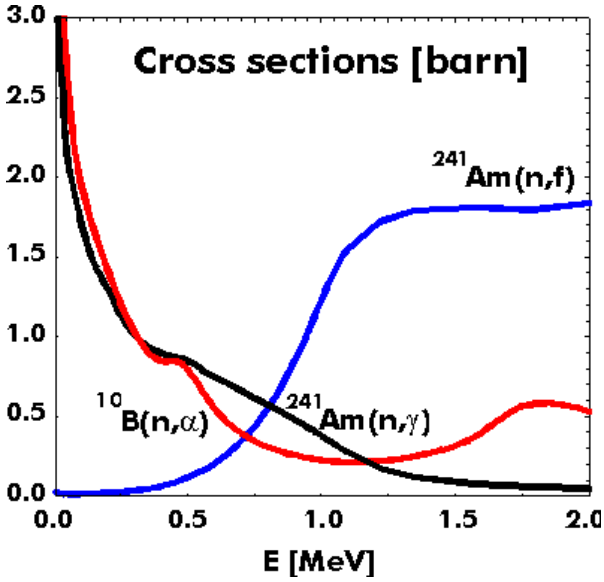

Figure 2-1. Absorption cross sesction of ^{10}B compared to the capture and fission cross-sections of ^{241} Am.

One drawback of introducing slow neutron absorbers into a sub-critical core is that source spallation neutrons have a softer energy spectrum than the average fission neutron, due to inelastic moderation in the spallation target. Hence, slow neutron absorbers tend to capture a larger fraction of source neutrons than of fission neutrons. To alleviate this problem the absorber was removed from the inner parts of the core during the design work. Accordingly, the minor actinides were also removed from the inner part, in order to maintain high fission to absorption probabilities of these nuclides. Replacing the absorber with a diluent (zirconium nitride) in the inner core could then be done without significant increase of curium production rates.

The finite range of the fission chain in sub-critical systems typically leads to high power peaking. Figure 2-2 exemplifies this fact for a simplified model of the ADS-design proposed by JAERI [12]. At a k-eigenvalue of 0.96, flux peaking (and hence for a homogeneously fuelled core power peaking) is as large as 2.0 already at beginning of the irradiation. Consequently the total power of the core, which is limited by the maximum allowable power in the "hottest channel", becomes low in comparison with what would be achievable for a critical configuration. In analogy with standard fuel zoning methods of critical reactor design, this problem can be addressed by differentiation of fuel to absorber or fuel to diluent volume fraction ratios over the core. The Sing Sing core geometry is shown in Figure 2-3. Each hexagonal ring of subassemblies corresponds to a fuel zone, counting from the innermost and outwards The diluent fractions in fuel zones one and two, and the absorber fractions in zones three to five were optimised for lead/bismuth and sodium cooled versions in order to obtain a radial power peaking less than 1.2 at BOL. The resulting fuel zone configuration for the sodium-cooled version is shown in Table 2-1, and the corresponding radial power distribution is displayed in Figure 2-4.

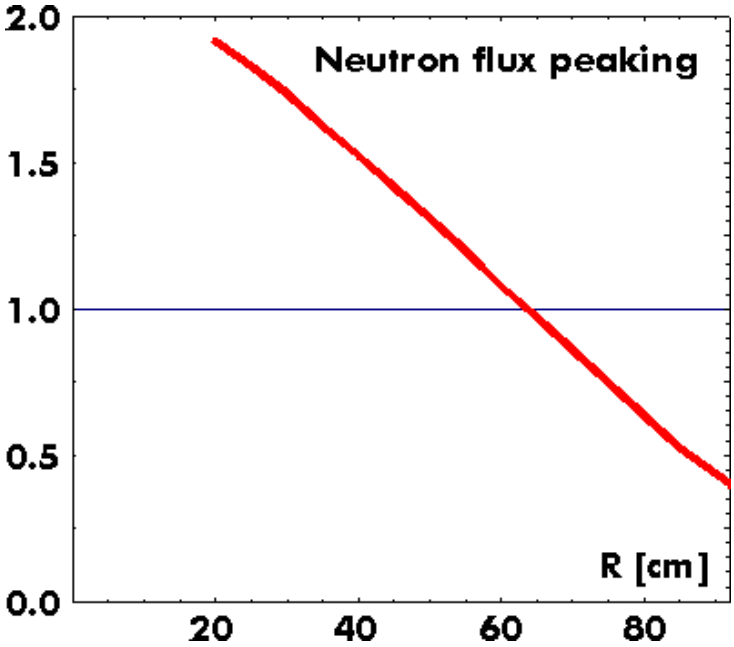

Figure 2-2. Radial neutron flux distribution in a homogeneously fueled subcritical core, similar to the design proposed by JAERI.

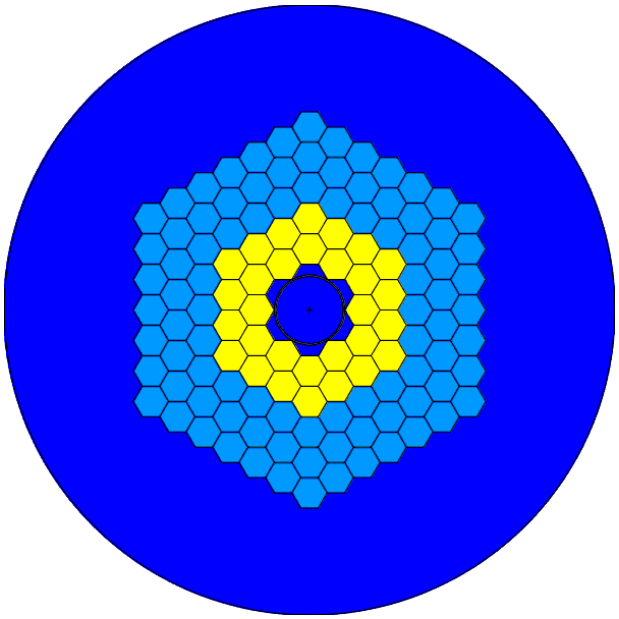

Figure 2-3. Cross section of the Sing Sing Core geometry. Yellow fuel assemblies contain (Pu,Zr)N fuel, blue assemblies contain (Pu,MA)N pins and B_4C pins. Dark blue central region – a spallation target, dark blue outer region – a coolant metal reflector. Each hexagonal ring of subassemblies corresponds to a fuel zone, counting from the innermost and outwards.

Table 2-1: Relative volume fraction of fuel, diluent (ZrN) and absorber (B_4C) in the Sing Sing Core, yielding a radial power peaking at BOL < 1.2. The minor actinides consist of 30% Np and 70% Am, corresponding to 30 years storage after discharge of LWR UOX fuel.

Zone	ZrN	B_4C	PuN	MAN
1	0.81	-	0.19	-
2	0.71	-	0.29	-
3	-	0.39	0.51	0.10
4	-	0.27	0.60	0.13
5	-	0.12	0.73	0.15

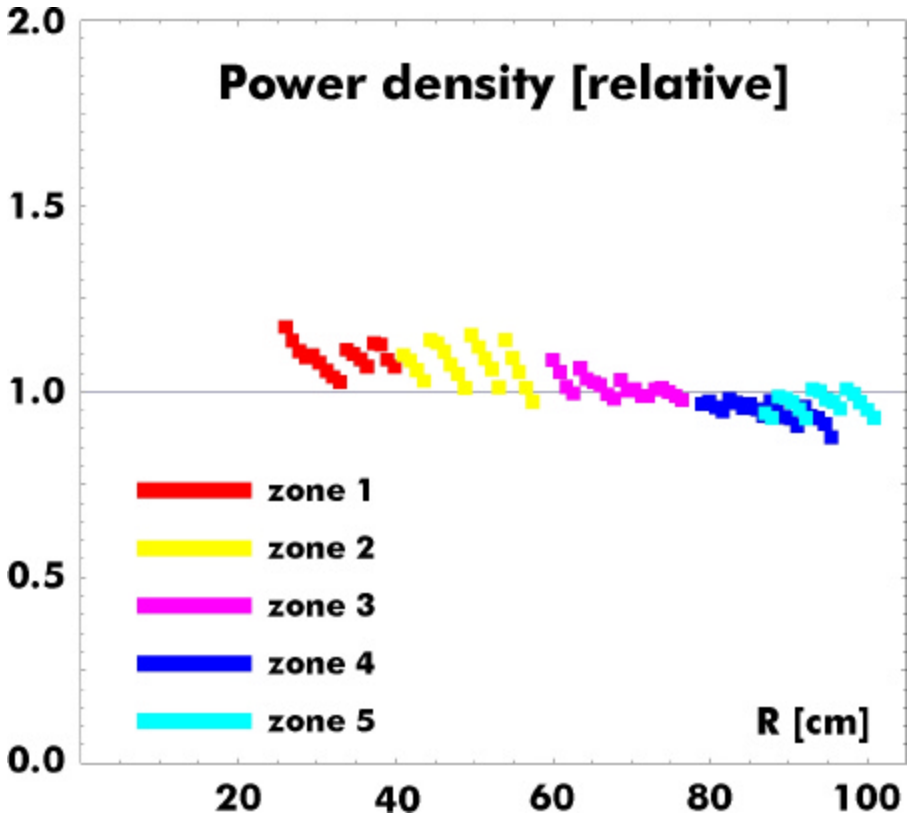

Figure 2-4. Radial power distribution in the Sing-Sing Core at keff ~ 0.96.

Nitrides were selected as the preferred fuel form, due to its potential of enabling a combination of high linear power and high burnup fraction. Figure 2-5 shows the relation between linear power and maximum fuel temperatures for oxides and nitrides assuming a typical fast reactor pellet geometry and a fuel surface temperature of 600 degrees C. The linear rating for oxides is limited by the melting temperature of americium oxide, which equals 2350 K. Hence $(Pu,Am)O_2$ fuels may not operate at more than 50 kW/m. The limiting factor for the nitrides is the dissociation of americium nitride, which takes place at comparatively low temperatures. The exact temperature dependence is unfortunately not know, but the successful fabrication of AmN in small quantities at JAERI [9] shows that AmN is stable at temperatures below 1600 K.

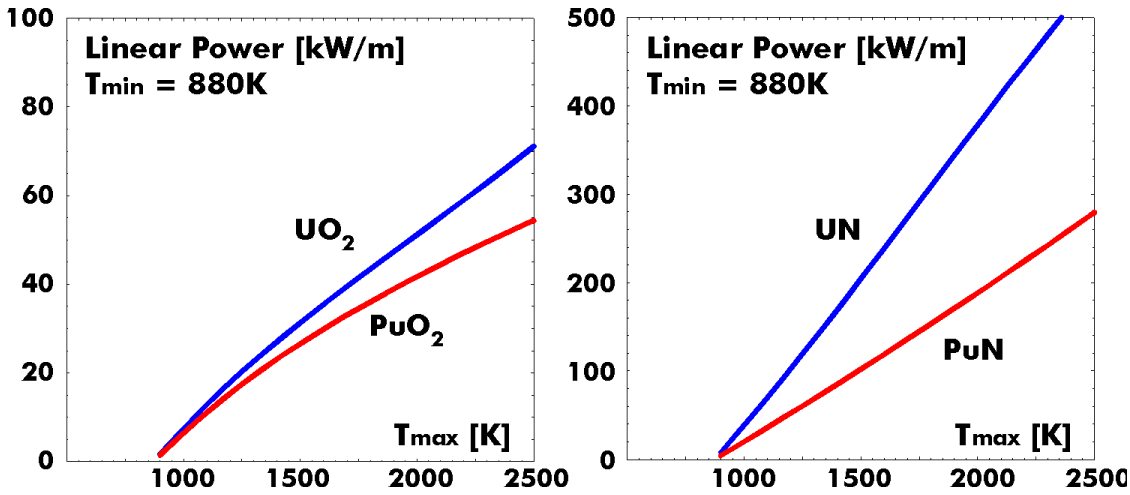

Figure 2-5. Linear power as function of maximum temperature for oxide and nitride fuels.

Adopting this temperature as the limit, and assuming that AmN thermal conductivity is similar to that of PuN, one finds that (Pu,Am)N fuels may operate at up to 100 kW/m.

The neutron absorber is introduced into the outer core zones as boron carbide pins distributed within the fuel assembly. The capture of slow neutrons in these pins suppresses the production rate of alpha emitting nuclides in the fuel. Consequently helium accumulation is reduced during irradiation, which improves pin performance as explained above. Further, (α,n) reaction rates during reprocessing become lower, with beneficial impact on costs for shielding. The resulting neutron spectrum in inner and outer parts of the Sing Sing Core is displayed in Figure 2-6. The corresponding fission to absorption probabilities for even neutron number nuclides are shown in Table 2-2. A comparison with values for fission probabilities in other core designs underlines the advantage of choosing the poison option as compared to the diluent option selected for the CAPRA, EA and JAERI designs of transmutation cores.

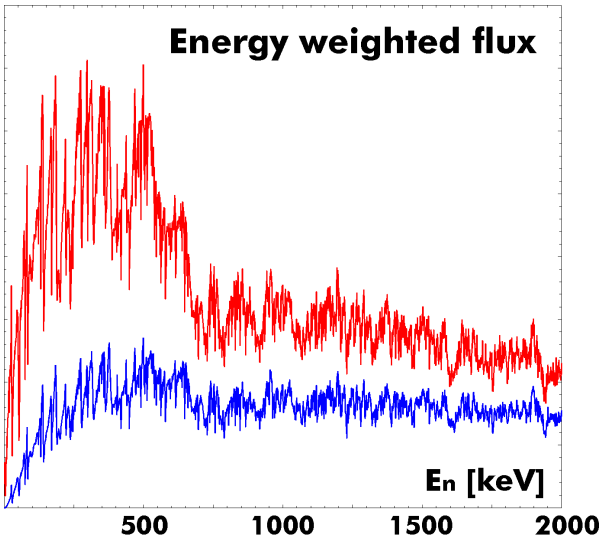

Figure 2-6. Energy weighted neutron flux distribution in inner and outer parts of the Sing-Sing Core.

Table 2-2: Ratios of fission to absorption cross-sections in different neutron spectra. SSC 1 & 4 denotes inner and outer core zones of the B_4C poisoned Sing Sing Core. The CAPRA project designed a critical sodium cooled plutonium burning core featuring 55% U-238 in addition to moderating inert material. In the Energy Amplifier of CERN, the Th to TRU ratio is 7/3, in order to maintain reactivity. A similar ratio of ZrN to TRUN is present in the Na cooled ADS proposed by JAERI, in order to obtain acceptable power densities.

Nuclide	SSC 1	SSC 4	CAPRA	EA	JAERI
Np-237	0.21	0.55	0.18	0.15	0.23
Pu-238	0.69	0.88	0.66	0.69	0.73
Pu-240	0.45	0.79	0.42	0.40	0.49
Pu-242	0.42	0.78	0.39	0.32	0.45
Am-241	0.19	0.43	0.14	0.12	0.16
Am-243	0.15	0.43	0.12	0.11	0.15
Cm-244	0.46	0.78	0.44	0.36	0.52

Note that the lead coolant adopted in the EA does not improve fission probabilities, in contradiction to claims of its designer. Rather than elastic scattering in the coolant, it is the macroscopic cross section of inelastic scattering on diluent materials that dominates the moderation of fast neutrons down to below the fission threshold of the even neutron number nuclides.

The choice of coolant in the design of reactors devoted to waste transmutation should be based on different criteria than those used for the Fast Breeder Reactor program. First of all, since the temperature feedback of the fuel is very small for uranium free fuels, the positive void coefficient of large sodium cooled cores leads to a deep sub-criticality requirement. In the JAERI design, voiding of the core results in a positive reactivity insertion of the order of 4000 pcm. Hence, the k-eigenvalue during normal operation should not exceed 0.95 in that case. Using lead/bismuth as a coolant greatly diminishes the void coefficient, since the tail of slow neutrons becomes much smaller. For cores based on the diluent option, void reactivity changes may even be negative. Therefore there is a large incentive to work on improving techniques of corrosion inhibition once developed in the Soviet lead/bismuth cooled sub-marine reactor program.

Due to the much poorer thermal conductivity of lead/bismuth, one needs to have larger mass flow of the coolant in order to be able to operate on high linear powers. Flow velocities of lead/bismuth are however limited to ~ 3 m/s in order to avoid erosion of corrosion protective films on structural material. Therefore one needs to increase the pin pitch to diameter ratios (P/D). This is to some extent incompatible with the requirements of FBR:s, since a larger neutron leakage deteriorates the axial blanket breeding potential. In transuranium fuelled fast reactors, however, the neutron economy is good enough for a high leakage not to be considered as an essential drawback. Figure 2-7 exhibits the heat removal capacity of sodium and lead/bismuth as a function of pin

pitch to diameter ratio. As seen, P/D = 1.3 is sufficient to keep maximum cladding temperatures below 1000K in oxide fueled sodium cooled reactors (maximum rating 80 kW/m), while P/D ~ 1.7 is required to remove 100 kW/m of linear power when using lead/bismuth coolant. Figure 2-8 shows a detailed 3-D thermal hydraulics calculation of the lead/bismuth temperature in a coolant channel being subject to a heat flux of 75 kW per fuel pin for P/D = 1.9 [11]. The margin to the lead/bismuth induced corrosion limit of 900 K appears to be sufficient.

Coincidentally a high P/D is also beneficial for the void reactivity coefficient. In sodium cooled cores this important parameter has a maximum at P/D = 1.5 [Khalil90]. The sodium cooled version of the Sing Sing Core (P/D = 1.5) accordingly has a voidworth of + 3460 pcm. Exchanging the coolant to lead/bismuth and increasing P/D up to 1.9 in order to maintain sufficient heat removal lowers this value to + 600 pcm, resulting in a comfortable margin to prompt criticality, even when setting the k-eigenvalue to 0.97 at BOL.

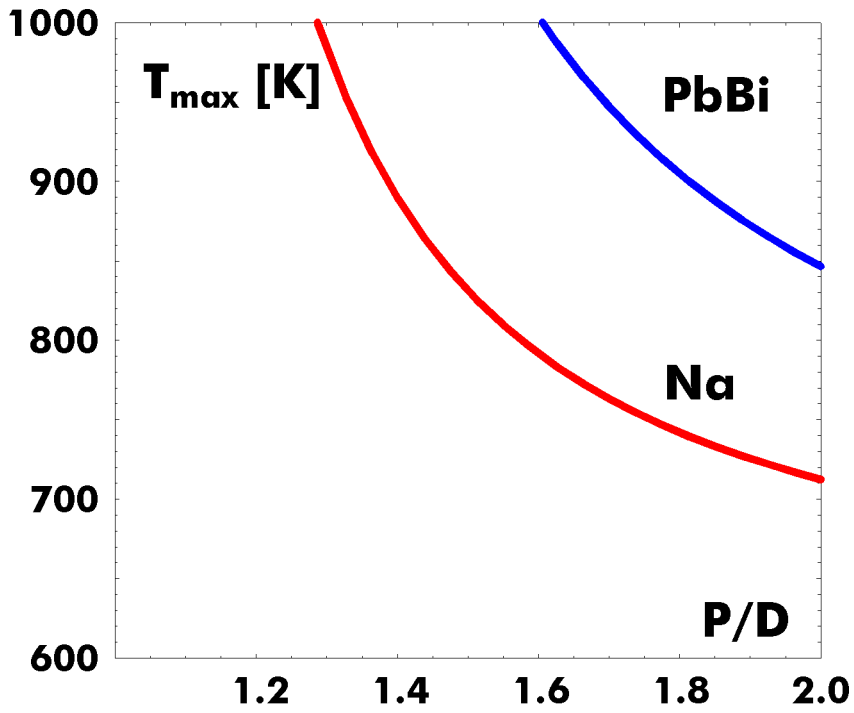

Figure 2-7. Maximum clad temperature as function of P/D for sodium cooling (red) and lead/bismuth (blue).

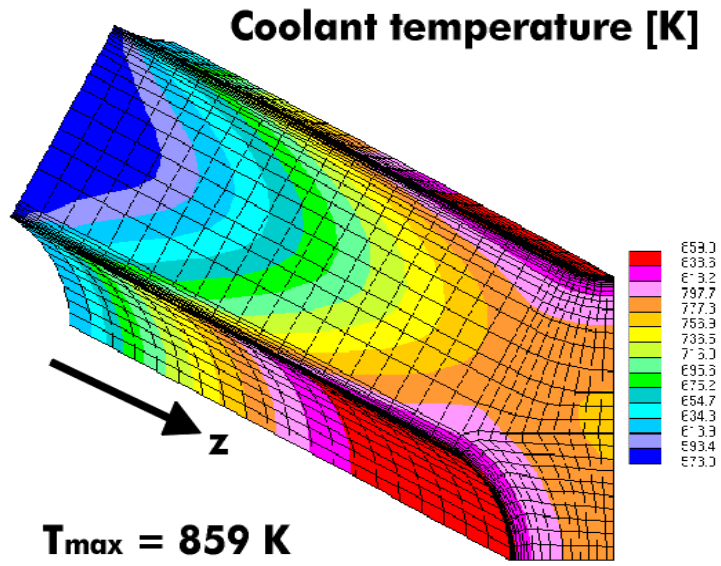

Figure 2-8. Temperature field in lead/bismuth for a pin power of 74 kW, an inlet velocity of 2.5 m/s and and an inlet temperature of 300^{o} C.

3 CODE DEVELOPMENT

Applications of Monte Carlo methods in radiation transport calculations using continuous-energy data have been growing along with a progress of computational power of computers. However, Monte-Carlo based burnup calculations with reasonable statistics are very lengthy and an average computational time required for these calculations is much larger (even by three order of magnitudes) than for stationary radiation transport calculations. So, effective Monte-Carlo burnup methods require dedicated numerical tools to perform a fast analysis of nuclide transitions in a transmutation phase space. The computer code that is under development at our Department code system is named MCB, as acronym of **M**onte **C**arlo Continuous Energy **B**urnup Code. It is a general-purpose code, which can be used for calculation of nuclide density evolution with burnup or decay, including k-eff calculations of critical and subcritical systems and neutron transport calculation together with all necessary reaction rates and energy deposition. The code integrates well known code MCNP, version 4B [14], which is used for neutron transport calculation, and a novel Transmutation Trajectory Analysis module (TTA) performing density evolution calculations, including formation and analysis of transmutation chains. Figure 3-1 presents a schematic flow-diagram of the MCB-code. The transmutation chain is represented by set of possible nuclide transmutation trajectories. The transmutation trajectory is defined as a sequence of consecutive nuclear reactions and decays that transforms one nuclide into another as a function of time. By solving a set of Bateman's equations describing concentration of the last nuclide of a trajectory, one can obtain analytical solution of nuclide concentration and the time integral of its destruction rate - called trajectory passage. Although, number of possible transmutation trajectories is infinite, one can put them into a series organized in an order of their formation as follows. Every trajectory after appending by a new possible reaction channel or decay path, forms a new trajectory that can be consider as a daughter trajectory of her parent trajectory and that way forming trajectory generations. Since the trajectory passage decreases with generation and it is greater than concentration of any of its daughter nuclide, it is used as a criterion for truncation of the trajectory series. This way the infinite family of trajectories is reduced to the limited series of meaningful trajectories contributing to nuclide density vector above a pre-determined threshold level. Trajectory formation and truncation process is performed on line using case dependent reaction rates. It represents more adequately the physics of the transmutation processes than a widely used matrix method.

MCB is compatible with MCNP and complete burnup calculation can be done in one single run that requires preparation of one input file, which can be slightly enlarged input of MCNP. The code uses extensive data libraries that covers nuclide decay schemes, continuous energy transport and reaction cross-sections, isomer state formation ratios, incident energy and target nucleus dependent fission product yield, and radioactive hazard indexes. This novel and advanced numerical tool can be used for a design of various nuclear systems, particularly in application to the accelerator driven systems. The first tests on the system were performed using the IAEA ADS-benchmark data covering both, time evolution of k-eff and transmutation of Tc-99.

Currently, the burnup-module is being integrated with MCNPX-code [15] in order to create a universal integrated tool for ADS simulations.

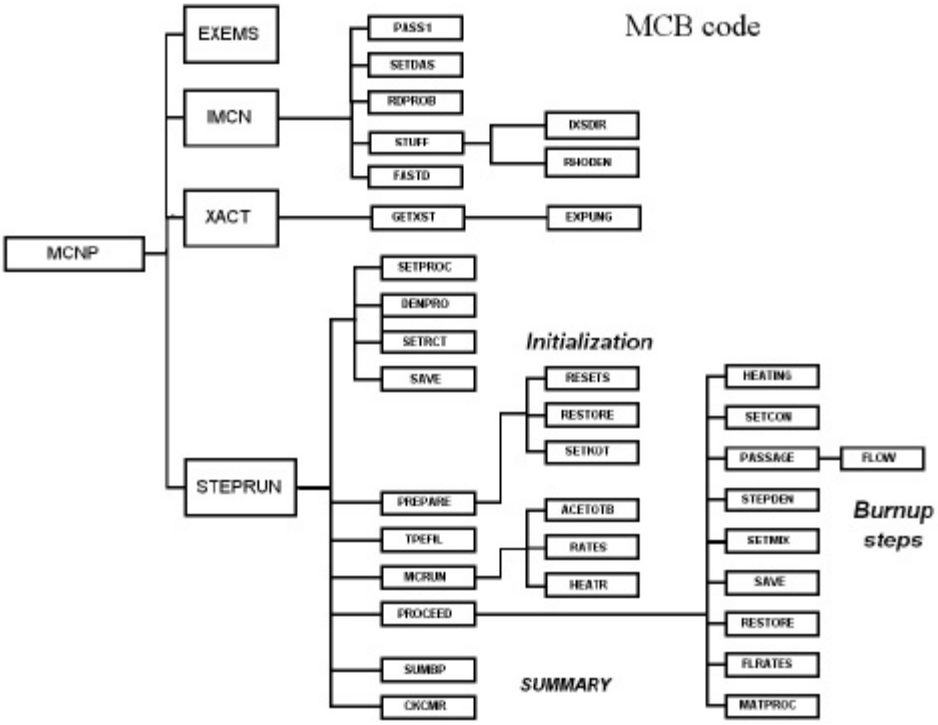

Figure 3-1. Flow diagram of the MCB code.

3.1 CODE FEATURES

System evolution with time of burnup is calculated according to system power or source strength in the user specified periods. The code supports calculations both, in subcritical system with external neutron source, and in critical systems where the neutron flux is adjusted to the required power.

The code is prepared to employ numerous cross-section libraries and data sets to adequately calculate reaction rates and nuclide formation probabilities. It includes possibility of separate treatment of cross section for different burnable zones to account for thermal effects, employment of energy dependent distribution of fission product formation, energy dependent formation of isomer nuclides.

Nuclide decay data is taken from two files. The first one TOI.LIB is prepared on the basis of Table of Isotopes and describes decay schemes for over 2000 nuclides. The second one XS.LIB is a decay data file used for ORIGEN code system [18] and it supports energy-integrated ratios of nuclide formation in excited state.

Reaction rates are calculated exclusively by continuous energy method with using transport cross-section libraries or dosimetry cross-section library. The user can specify libraries explicitly or by using default option scheme for library definition that is an extension of the scheme used in MCNP. It allows the user to assign different library to different cells for the same nuclide if needed.

Formation of nuclides in excited states due to neutron capture or (n,2n) reactions is supported by XS.LIB file while energy dependent isomer formation ratios can be taken from file ISB.LIB.

Energy-dependent fission product yield is calculated automatically according to the specification and the data in the FY.LIB that contains energy distributions of fission products for every fissionable nuclide.

Heating is calculated automatically during burnup calculations if data with heating cross section are present in the library. In other case, or if required, the user can use an option to calculate heating from fission only.

Time evolution of nuclide densities is calculated with the complete set of linear transmutation chains that is prepared for every zone and time step so it is adjusted to evolving transmutation conditions. The code uses Bateman method to solve, prepared-on-line and complete, set of linear chains that noticeably contribute to nuclide formation.

Dose of burnable material is calculated on the basis of EURATOM Directive [17].

The program calculates neutron multiplication of the external source and the fission source as well as neutron multiplication factors. They are used to calculate source importance defined in two ways. The first one is for fission generation and the second one is for neutron multiplication. Time evolution of those parameters together with neutron source strength, energy deposition per source neutron and potential dose and activity of material is printed out.

Self-adjusting step routine is available when the user defines allowed variation of k_{eff} or heating. Other control parameter can be used to switch mode of calculation from external source to fission source (k-code) when current value of k_{eff} reaches specified level.

Program calculates transmutation transitions from nuclide to nuclide and prints them out to one of the output file. Transmutation chains that are formed by the code can be also printed for interesting nuclides.

3.2 CROSS-SECTION LIBRARIES AND DATA FILES

In order to provide accurate transmutation calculations the code must be supported with data files, which allow for complete simulation of neutron transport and nuclide formation. The bulk of data consist of numerous cross-section libraries for calculation of reaction rates and transport cross-section library. The scope of neutron libraries distributed with MCNP package is limited and lucks libraries for many nuclides, so it is recommended to use an enlarge set of cross sections. Other problem considers number of available reactions. Since standard transport library does not contain some reactions, it is recommended to supplement this data from dosimetry libraries to complete the reaction list. In order to fulfill above recommendation the code is designed to employ simultaneously, transport and dosimetry libraries for every material.

Second part of data files concerns nuclide formation processes and radioactive nuclide properties. The decay schemes of over 2400 nuclides, including metastable, were prepared on the basis "The Table of Isotopes 8E" [16] while the dose data of 738 nuclides were prepared on the basis of Euratom Council Directive 96/29/EURATOM [17]. The data file TOI.LIB contains the data describing decay constants with branching ratios, and the values of committed effective dose per unit intake.

Since formation processes of isomer nuclides is not well treated in existing libraries of MCNP as well as in "Table of Isotopes" we need to get necessary data from other sources. The first one is the one-group cross-section library of ORIGEN, which serves for calculation of isomer formation ratio due to decay, reaction (n,2n) or neutron capture. It is attached to the program as XS.LIB file.

Since the ORIGEN file supports only average energy data, for some important cases we have prepared energy-dependent isomer formation ratios making ISB.LIB file. Currently available file contains formation ratios of ^{242m}Am and ^{244m}Am based on Mann & Schenter model [19].

Incident energy and nuclide dependent fission product yields were prepared based on Wahl [20] model. Produced file FY.LIB contains fission product yields functions for 36 heavy nuclides.

3.3 INPUT AND OUTPUT FILES

MCB input file can be made from standard MCNP input file by addition of few cards that will define transmutation system. However in order to describe some complex cases optional material definition have been introduced.

3.4 TRANSMUTATION SYSTEM DEFINITION

The MCB code can work as a standard MCNP unless burnup option is switched on. The card BURN that contains the list of burnable material does the switch. In the burnup mode the code takes control over user specification of the transmutation condition and gives warning messages in case of user error of specification. Obviously program does not perform full checkup of physical consistency of the system definition but checks consistency with program requirements to complete calculations. Without BURN card MCNP mode is used and all other burnup control cards are simply ignored but new option of material definition remains valid. The user can use this feature in case of run trouble to check out if problem lays in system definition for MCNP or for burnup. In order to properly set up the problem the user need to introduce specification of:

- burnable material,
- libraries required for reaction rates calculations,
- duration of transmutation time periods,
- system normalization with external neutron source strength or thermal power.

3.5 MATERIAL AND LIBRARY DEFINITION

MCB requires much extensive number of materials handling that results in necessity of improving (simplification) material specification from the user point of view as well as material differentiation in order to avoid unnecessary data processing. Since calculation process is much more complex than in case of pure MCNP the material and libraries should be differentiated. Different treatment is required for abundant materials that influence the neutron transport process and for low abundant material. Moreover, the case is fluent when with transmutation some nuclides disappear while others emerge.

Therefore for burnup case libraries for all possibly emerging nuclides must be specified. The material and library definition can be done for such a case with usage of extended material definition option design for MCB, that is by usage of combination of M, MB, MR, and MIX cards

Following three categories of material are defined:

i) Transport material - is used in particle transport simulations and also in remaining calculations. It is specified on M card and obviously has its density and assigned library.

ii) Burnup material - is not used in transport calculation unless its density accumulates to a certain level, at which its cross section contribution to the total cross section of the cell materials reaches a discrimination level. In such a case the material is ranked-up to the transport material. It is specified on MB card and assigned library is used for calculations of reaction rates.

iii) Residual material - has no defined density and is used only for transmutation transition calculations, so it cannot diminish from the system due to burnup. It does not contribute to the buildup of other nuclides unless it has accumulated as a daughter nuclide due to the burnup. Residual material can be used also for specification of cross-section library for zones when the nuclide is absent at BoL.

The mixing of several materials defined by cards can be done with a MIX option. The mixing option can simplify system definition also for MCNP since a material can be made of its component material, and not only directly of nuclides.

The MIX option can be also used for cross-section library hierarchy definition. This option was prepared for cases when cross-section libraries of nuclides used in the system has different id numbers and it would be tiresome to specify them all directly. Hierarchy list works in a natural way - the cross section table with highest position in the list will be loaded. Lack of the hierarchy list, even for one entry, results in loading only those cross-section libraries that are directly or by default specified for transport. It means that nuclides absent at BoL but emerging, as transmutation products will have no cross sections loaded. This can produce incorrect results.

Appropriate system definition requires that for every burnable material the library hierarchy list should be formed. There are possible cases when the user does not accept some nuclide cross-section and needs to replace this by other library cross section. In such case the required nuclide library should be specify directly in one of material cards for burnable material.

The library hierarchy list is also required when the user needs to use both transport library and dosimetry library to support full available list of reaction. Since one nuclide cannot appear twice in the material list it is the only way of using both data libraries.

Other problem appears with metastable nuclides since in case of MCNP libraries there is no distinction between isomers. It is solved by making a new convention of isotope identification, so called ZAID number definition. When a ZAID number represents mass number greater than 300 it is treated as isomer excited state of nuclide. This form of ZAID should be made at the cross section preparation process and XSDIR file should

contain it. However since in old libraries ^{242m}Am is represented like a ground state nuclide usage of old libraries would be not proper. For such cases the user can use special option (GTMET) assigning ground state libraries also to the metastable isomer. Additionally, the user can use substitutes of ZAID that is ZA replaced by nuclide or element chemical symbols, in order to simplify material recognition. Currently substitutes of the following form are legitimate:

- Pu239.55c for 94239.55c
- Pb.55c for 82000.55c
- U235 for 92235
- Pb for 82000
- Am242m for 95342 etc.

3.6 MODES OF CALCULATIONS

Burnup calculations can be done either in a k-code mode or a source mode. This means that reaction rates are calculated in one of the modes. Also it is possible that system switches between two modes depending on current value of k_{eff}. In both cases if user wishes to control level of k_{eff} the k-code mode must be used for this purpose. There are few possibilities:

- Lack of KCODE card will result in omitting k_{eff} evaluation and program will make burnup only in transport mode and can accomplish calculations providing system remains subcritical.
- If the user requires using only k-code then a switch parameter should be put to 0.0. In such a case system will never switch to source mode and will not be able to calculate normalize flux and consequently power of the simulated system must be given explicitly.
- Switch parameter controls the choice of calculational mode between k-code and source-mode.
- For time steps with thermal power and source strength set to zero the burnup is calculated as a natural decay and no reaction rates are need to be calculated.

3.7 BENCHMARKING OF THE CODE

First extensive tests of MCB code were performed in the frame of NEA/OECD benchmark [12] and the final results of this benchmark are still under extensive processing. In this benchmark a simple, predefined model of ADS with fast neutron spectrum and Pb/Bi coolant has been simulated - see Fig. 3-2 – by 6 research groups in order to compare the results of calculations and eventually, to understand the discrepancies. As the only code in this benchmark, MCB was used for simulations using 3 nuclear data libraries: JEF2.2, ENDF/B-6.4 and JENDL3.2, which was very helpful in identifying discrepancies originated from differences in nuclear data libraries for cross-sections of Pb. This was the case of ANL-calculations as presented on Fig. 3-3.

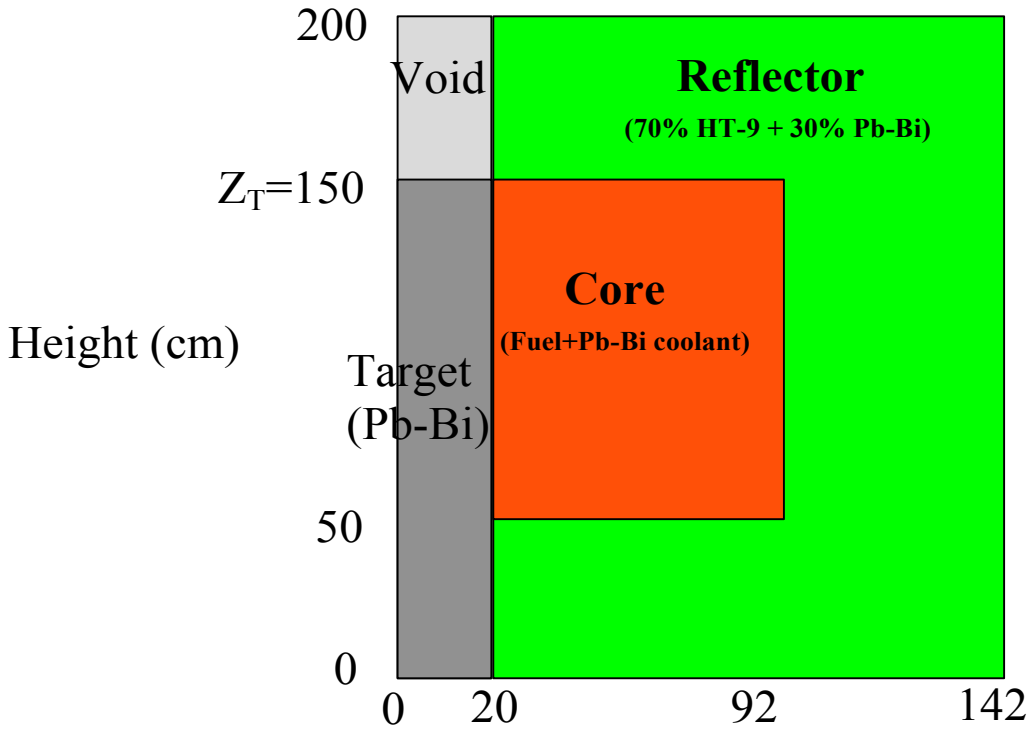

Figure 3-2. A simple, cylindrical model of ADS for a NEA/OECD benchmark. The model comprises a central pb/Bi target zone, a void zone in the beam duct region, a multiplying region consisting of homogenised fuel and Pb/bi coolant, and an outer steel reflector zone. The core dimensions are those of the ALMR burner reference core.

Figure 3-3 demonstrates clearly the quality of MCB-results: k_{eff} evolution with time in a start-up, obtained with MCB (a curve marked RIT) is very close to the average results. The same pattern can be seen on Fig. 3-4 where k_{eff} evolution with time for equilibrium ADS core is presented.

Finally, Fig. 3-5 presents the neutron spectrum for the start up core. Again, the agreement of MCB results with other codes is remarkably good. The lowest energy group, which differs visibly from other results, was deliberately averaged over a much broader energy range than in other calculations.

The OECD/NEA benchmark results can be treated as an important validation step for the MCB code and after introduction of new features enabling parallel processing, MCB will be released for the research community through the NEA-Data and Program Library.

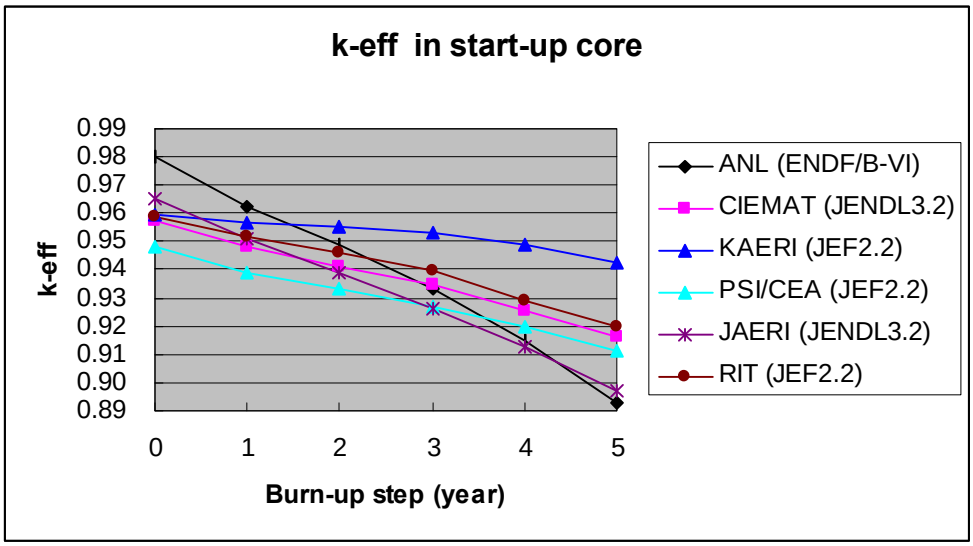

Figure 3-3. k_{eff} variation with burnup in start-up core

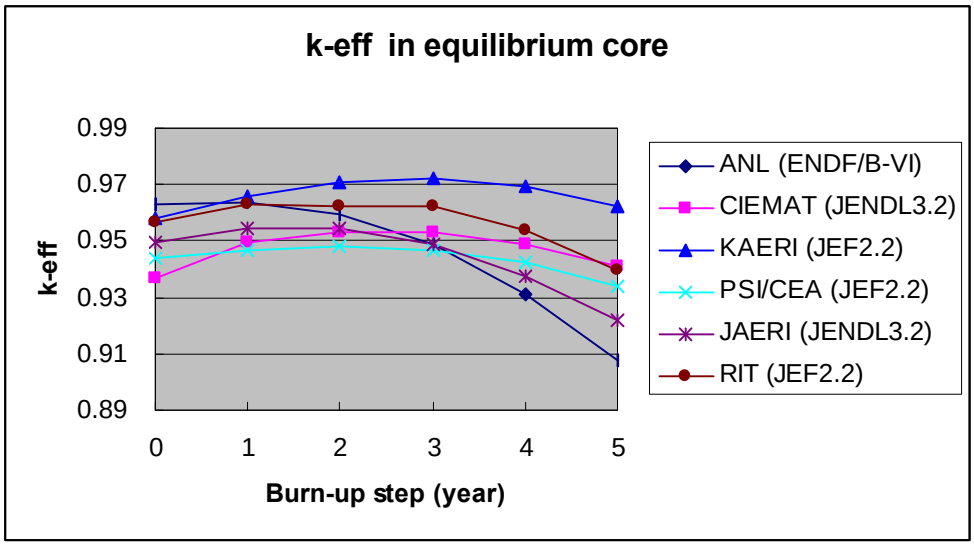

Figure 3-4. k_{eff} variation with burnup in an equilibrium.

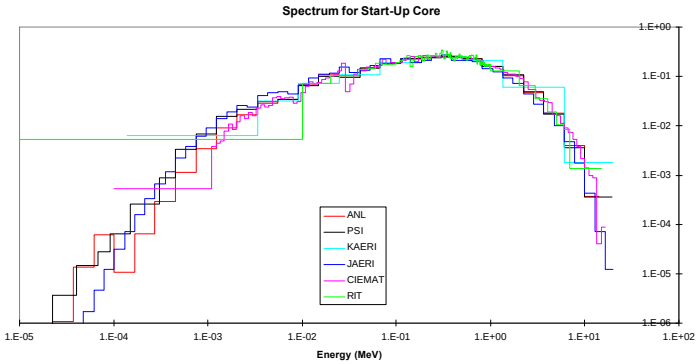

Figure 3-5. The neutron spectrum of a start-up core.

4 SUB-CRITICAL DYNAMICS ANALYSIS

The accelerator-driven systems may have some extraordinary safety potential as well as a reliable means for power control. However, this has to be proven in detail and so far few analyses have included advanced dynamical models of how accelerator-driven waste transmutation systems behave under operational and transient conditions. Sub-critical reactors do not respond dynamically in the same way that ordinary nuclear reactors do. A simple relation offers insight into the fundamental difference between a sub-critical and a critical reactor:

$$P \propto S/\rho$$

The power level, P, in a source-driven system is proportional to the source strength, S, and inversely proportional to the reactivity, ρ, 0. The source may be subject to control as a means of adjusting the power level of the system while the reactivity is constant. The response of the system by perturbing the source strength is amplified as the reactivity approaches zero. For example, if the reactor is close to critical a small change in source power will have a large impact on the system power. Which represents a significant difference from a critical system, where the reactivity and the source is zero, and the power level is set by changing control rod position or by changing the feed water flow-rate like in BWRs. In a traditional reactor the reactivity is nonzero during transient conditions, however, thermal and hydraulic feedback effects will force the reactor back to critical conditions. The neutronic response time is determined by the half-life for decay of delayed neutron precursors. For a source-driven system with a large degree of sub-criticality, the delayed neutron precursors do not appreciably slow the response of the system [22]. The source dominates the system and the power response to a perturbation is almost instantaneous.

Very few if any simulation tools for analyzing advanced dynamic problems in sub-critical fast reactors exist. An important reason for this lack in simulation capability is that most existing time-dependent codes describes a reactor system without external neutron source. However, the neutron distribution in an accelerator-driven system follows the source-driven inhomogeneous reactor solution [23]. When an inhomogeneous system is near critical there will be little deviation between the source-driven distribution and the corresponding homogeneous fundamental eigenmode. When inhomogeneous systems are far from critical their neutron distributions may differ significantly from the corresponding fundamental eigenmode.

Apart from analyzing well known transients such as Loss of Heat Sink, Loss of Flow, etc. the accelerator-driven system must be investigated subject to beam-off and beam-on conditions. According to Burns and Rydin [24], the neutronics response of a deeply sub-critical ($k_{eff} \sim 0.95$) system to a source variation is almost instantaneous. Hence, a beam-off/on situation produces an instant power transient in the reactor. The effects of such transients must be investigated under short- and long term conditions since a large number of thermal cycles induce fatigue effects in steel components. Some preliminary results have recently been presented [24][26]. In both analyses the time behavior of coolant temperatures in critical regions of the system following a beam interruption has been calculated.

In [24] a core-dynamics analysis has been carried for an 80 MW Energy Amplifier Prototype fuelled with MOX and cooled by a molten lead-bismuth alloy. The results were obtained by a dynamics code developed at ENEA by coupling single channel thermal-hydraulics and point kinetics. During the transient a constant flow rate was assumed. Figure 4-1 shows the outlet coolant temperature in case of a beam interruption event.

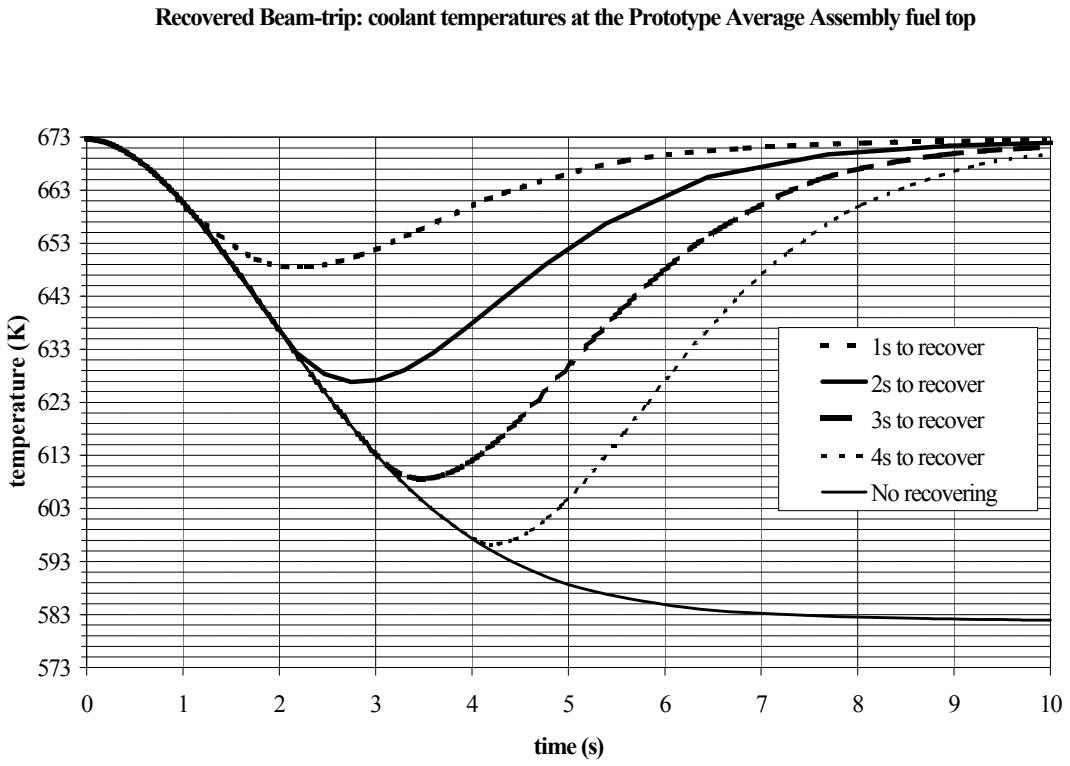

Figure 4-1.Coolant temperature transients during the Beam-trip and recovered bean

The outlet coolant temperature reaches the inlet temperatures (»573 K) within 10 seconds if the beam is not recovered. About 30 seconds after the trip, a further drop in coolant temperature of about 50 K will start resulting from the transit of primary-coolant at lower temperature through the heat exchanger to the inlet channel. Hence, unmitigated beam interruption events lead to a total drop in temperature of the core-outlet coolant of about 150 K. Included in Figure 1 is the temperature drop relevant to the recovery of the nominal beam intensity. It is seen that a beam interruption that is recovered within two seconds would induce a drop in temperature lower than 50 K. Moreover, all recovered beam trends show that outlet coolant nominal temperature would be restored in 10 seconds. Owing to this reset of the outlet coolant temperature, the previously mentioned second drop in temperature (that occurs about 20 second later) would not superpose itself to the first one.

In [26] the SASSYS-1 code is used to calculate transient coolant and structure temperatures in an Accelerator Transmutation of Waste device using a sodium cooled configuration modelled on the Advanced Liquid Metal Reactor (ALMR). Changes in reactor power level are computed with point kinetics. The transient is a beam interruption which drops the power from full power to zero in 1 microsecond at the start of the transient. Cases are run both with and without a trip of the pumps when the beam

interruption occurs. The reactor k_{ef} is 0.975. A 12 channel thermal hydraulics model is used for the reactor core, and a detailed treatment is used for the primary and intermediate heat transfer loops. The nominal core temperature rise is 139 K, and the temperature rise in channel 1, the hottest channel, is 164 K. The coolant transit time through the core at full forced flow is 0.2 second. The transit time through the upper part of the subassembly above the core is 0.3 second, and the transit time through the outlet plenum to the intermediate heat exchanger (IHX) inlet is 51 seconds. Considering a beam loss with no pump trip the temperature of top of core coolant drops rapidly and approaches the decay heat curve, see Figure 4-2.

The results are for the above core load pad. Upon a sudden drop in source, the power density and fuel temperature respond immediately, followed by the cladding temperature. The coolant temperature initially drops faster than the structure temperature. However, since sodium has very high thermal conductivity, the structure temperature is almost the same as the coolant temperature. The bulk structure temperature responds more slowly at a rate determined by the structure thickness, thermal conductivity, and heat capacity. The difference between the bulk structure temperature and the coolant temperature is given in Figure 4-2. This difference peaks 2.2 seconds into the transient at a value of 88.6 K. Thus, any beam interruption longer than 2 seconds is going to give a thermal stress corresponding to almost 90 K at the above core load pads.

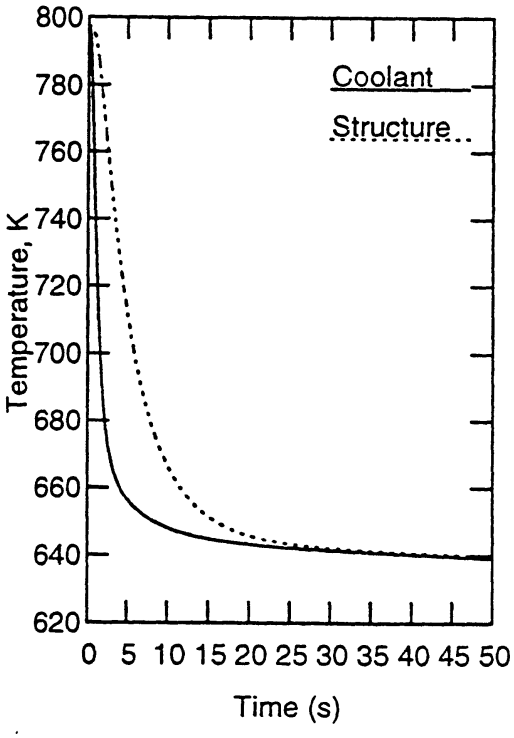

Figure 4-2. Top of Core Coolant and Structure Temperature. No pump trip [6].

Both analyses [24][26] have illustrated the safety problem of numerous beam interruptions, however, both models must be further developed. The first and the most important task is to incorporate space-time neutronics. It is a general opinion [27] that spatial effects in large metal cooled reactors are an important issue that must be investigated separately.

5 EMERGENCY DECAY HEAT REMOVAL BY RVACS

Emergency decay heat removal by a Reactor Vessel Auxiliary Cooling System (RVACS) is required in a Loss-of-Heat Sink (LOHS) accident in which the normal heat removal means are not operational e.g. due to a station blackout. The latter would mean that also the accelerator and the primary pumps are switched off (i.e. additionally a Loss-of-Flow – LOF - condition). It is also conceivable that the primary and secondary pumps loose their power supply and that the accelerator is not switched off. After a beam-stop, the power will decrease to decay heat level which will, initially be about 6.7% of the normal operating power [28], but it decays exponentially with time.

The RVACS is a totally passive system i.e. neither human operations nor mechanical devices are necessary to initiate them. Only physical laws (like heat convection and gravitations) govern an RVACS, which makes it extremely unlikely that it fails to operate. The physical foundation for the RVACS is the temperature difference, and consequently the density difference between the air in the downcomer relative to the riser of the RVACS. Due to the heat-up during the LOHS accident a static pressure difference develops, which sets the air in motion and leads to heat removal.

So far most of the analysis on RVACS was related to sodium-cooled reactors. Since future ADSs will probably use Pb/Bi cooling, new calculations using this coolant are needed. The thermo-physical properties that are important for heat removal by natural circulation such as thermal expansion, viscosity and thermal conductivity are quite different for Pb/Bi from those for sodium. It is important to determine the maximum thermal power of an ADS for which the decay heat can still be safely removed with an RVACS.

It is also important to investigate different options for increasing the heat removal such as different emissivities, the use of ribs and fins. Some more investigations on different rib and fin configurations and pitches appear still necessary.

For the ADS it is also of interest to study the decay heat removal for LOHS accidents in which the proton beam is not switched off soon after the accident initiation. Such analyses will give the times available for shutting off the accelerator before some fuel or structural damage will take place.

In situations like the one mentioned above or for higher power systems, extra heat removal means are very attractive since they both decrease the maximum coolant temperature and reduce the amount of time the coolant remains at elevated temperatures.

An analysis of RVACS on the Energy Amplifier (EA) and RVACS on the Power Reactor Inherently Safe Module (PRISM) and the Reactor Auxiliary Cooling System (RACS) on Sodium Advanced Fast Reactor (SAFR) has been performed based on the published results identifying further research needs.

A computer code for thermal hydraulic calculations - STAR-CD has been validated for natural convection modelling by comparing against the experimental results of the PASCO facility at FZK [29]. Then a parametrical study on a simplified geometry of an

RVACS has been performed. Finally, an RVACS has been analysed for the emergency decay heat removal during an LOHS in 80MWth and 800MWth ADS, respectively.

5.1 VALIDATION OF STAR-CD FOR NATURAL CONVECTION FLOWS

As an example of STAR-CD validation results for a Two-Layer Model are presented. This model employs a low Reynolds number formulation on a fine mesh within the boundary layer close to the walls and a high Reynolds number model is used in the free-stream on a coarser mesh [32]. In order to resolve the heat transfer properly, at least 15 cells next to the wall surface are necessary.

In the PASCO facility, the air has to pass an inlet bend of 90º angle in relation to the test channel. Vanes are used to steer the flow into the channel as smoothly as possible. The STAR-CD simulation takes this into account as an additional pressure loss, added to the channel inlet. The pressure loss is calculated analytically as [35]

$$\Delta p = 4 f \frac{L_e}{D} r \frac{V^2}{2}$$

For a 90-deg elbow of medium radius, the L/D is chosen to be 26, thus the pressure drop is 2.01Pa for a velocity of about 1,25m/s and friction factor of 0.026 for a smooth surface. When the pressure loss is included, the Star-CD calculations predict a mass flow of 0.37kg/s and a heat removal rate of 6700W. The calculated velocity profile is shown in Fig. 5-1, and the temperature profile in Fig. 5-2.

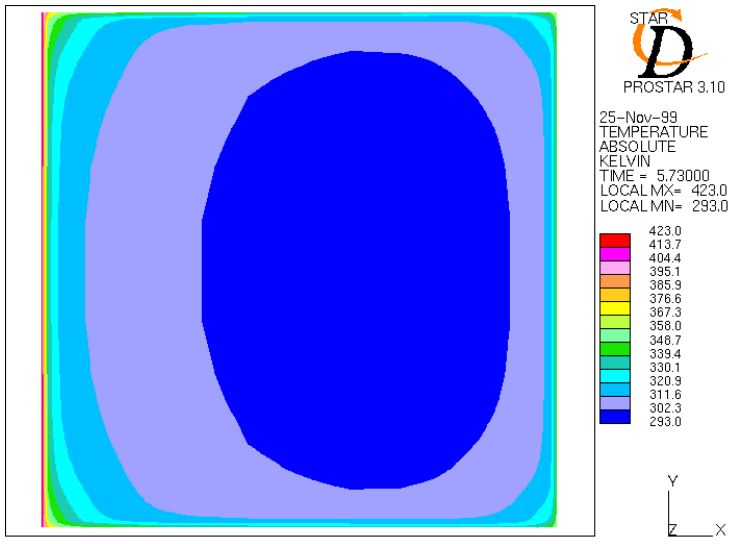

Figure 5-1. The velocity profile at outlet of the PASCO channel calculated with STAR-CD

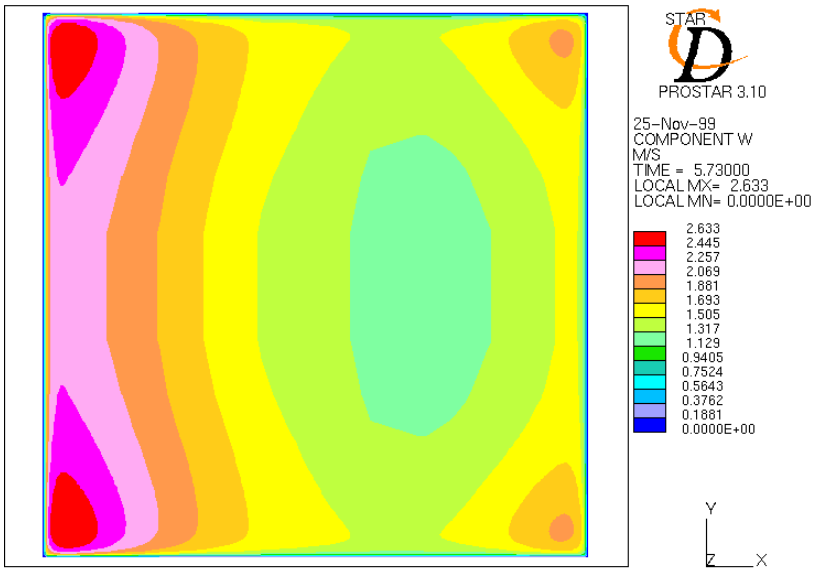

Figure 5-2. The temperature profile at outlet of the PASCO channel calculated with STAR-CD

5.1.1 Heat transfer correlations

Examinations employing wall functions in the boundary layer have also been performed. These models usually give less accurate estimates, but are less expensive regarding computational time. Several heat transfer correlations were investigated. The correlation showing best agreement with the experimental results was developed at the Argonne National Laboratory (ANL) within the American Liquid Metal Reactors' (ALMR) program [36].

$$Nu = 1{,}22 * \mathrm{Re}^{0.456}\,\mathrm{Pr}^{0.4} \qquad (2)$$

This correlation predicted a mass flow rate of 0.355kg/s and a heat removal rate of 6600W. This is to be compared with the standard heat transfer correlation in STAR-CD, which calculated a mass flow of 0.361kg/s, and a heat removal rate of 6994W. The temperature and velocity profile can be seen in Figs 5-3 and 5-4, respectively.

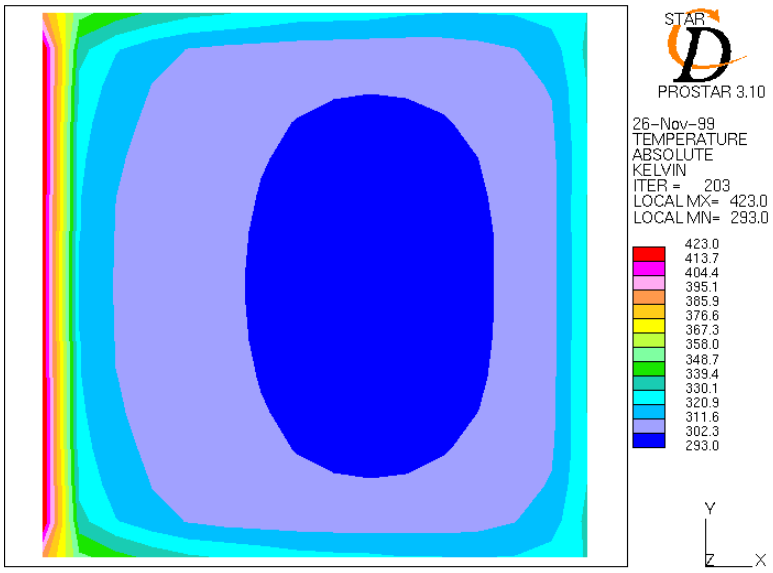

Figure 5-3. The velocity profile at channel outlet calculated with STAR-CD using the heat transfer correlation of ANL.

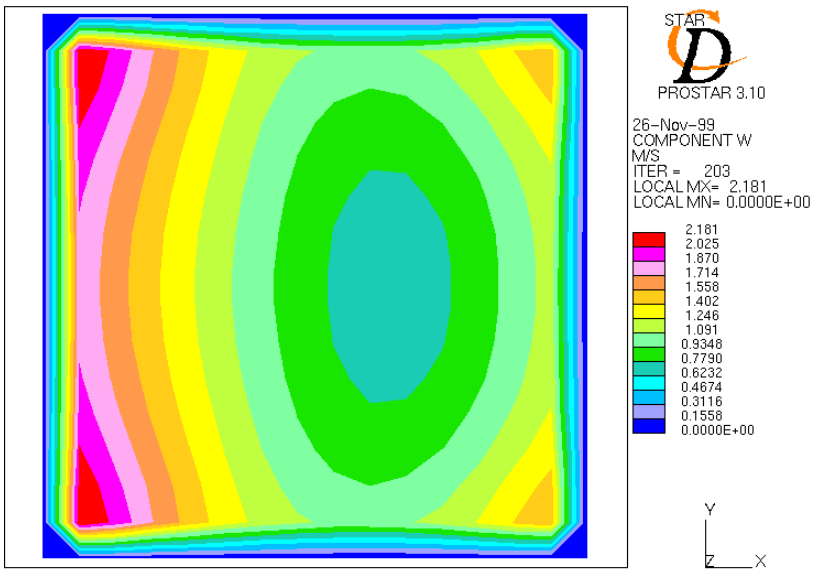

Figure 5-4. The temperature profile at channel outlet calculated with STAR-CD using the heat transfer correlation of ANL.

5.1.2 Conclusions from the Validation Calculation

The comparison of the STAR-CD calculations with the Pasco results has two important aspects. First the STAR-CD code can properly simulate this experiment with its detailed two-layer model for the mass and heat transfer in the hydrodynamic and heat transfer boundary layers. However, for the practical application of a CFD code such as STAR-CD, it is of key importance to use coarse meshes together with appropriate heat transfer correlations. The ANL correlation showed very good agreement with the PASCO

experiment, which is not surprising since it was developed for natural air circulation at high temperatures within the ALMR program. The heat and mass flow was over predicted by 1.5% compared to the PASCO experiment.

5.2 PARAMETRICAL STUDY

Parametrical studies were performed on a simplified geometry, representing only the RVACS air channel similar to the PRISM and SAFR design. One parameter at a time was examined in order to find its influence on the air mass flow and the heat removal capacity. The calculations were performed on a coarse mesh using ANL's heat transfer correlation, Eq. 2. This was employed in all calculations except the surface roughness study where the Two-layer model was used.

A reference case was chose to have a surface emissivity of 0.75, and a hydrodynamically smooth surface roughness. Furthermore, no fins are used and the guard vessel temperature is kept at 773K. The gap width between the guard vessel and the collector wall is 18cm.

The studies comprised:

- The surface emissivity
- Surface temperature
- The surface roughness
- Fin pitch on guard vessel
- Gap width between guard vessel and collector wall

5.2.1 Conclusions of the Parametric Study

From the parametrical study it can be concluded that a change of emissivity from zero to one doubles the heat removal. The heat removal is found to be more than triple when the wall temperature is increased from 573K to 973K. The surface roughnesses of the guard vessel and collector walls have a small impact on the heat removal. The optimal fin pitch regarding the heat removal was found to be between 5cm and 10cm, where the heat removal was twice compared to the case without fins. The results on optimal fin pitch have not been found in the literature concerning RVACS. At last it was found that if the gap between the guard vessel and the collector wall is increased from 10cm to 60cm, the heat removal increases by about 15%.

5.3 LOSS-OF –HEAT SINK AND LOSS-OF-FLOW CALCULATIONS BASED ON 80MW$_{th}$ ADS DESIGN

5.3.1 Ansaldo's proposal of a demonstration design

The demo design of Ansaldo [31] has been used in the investigation of the decay heat removal by an RVACS. In Fig. 5-5, the geometry of the pool-type design can also be seen. The height of the reactor vessel is about 8m and the inner diameter is 6.0m. A

cylinder inside the reactor vessel of 2.6m diameter separates the riser and the downcomer. The separating cylinder reaches from the core bottom, until 30cm below the surface of the Pb/Bi coolant. The core is located at the bottom of the riser, its height is 1m and the power generation is 80MWth during normal operation. Above the core inert gas is injected in order to increase the nominal flow rate. The heat exchangers are located at the top of the downcomer in the reactor vessel. A modified model of this type was then designed for a power of 800MWth.

A guard vessel is surrounding the reactor vessel and represents an extra safety barrier in case of a break of the reactor vessel. Both vessels are separated by an air gap of 20cm width, which also serves as an insulating layer during normal operation. The RVACS considered in this thesis is based on the design of the American Liquid Metal Program (ALMR) [42].

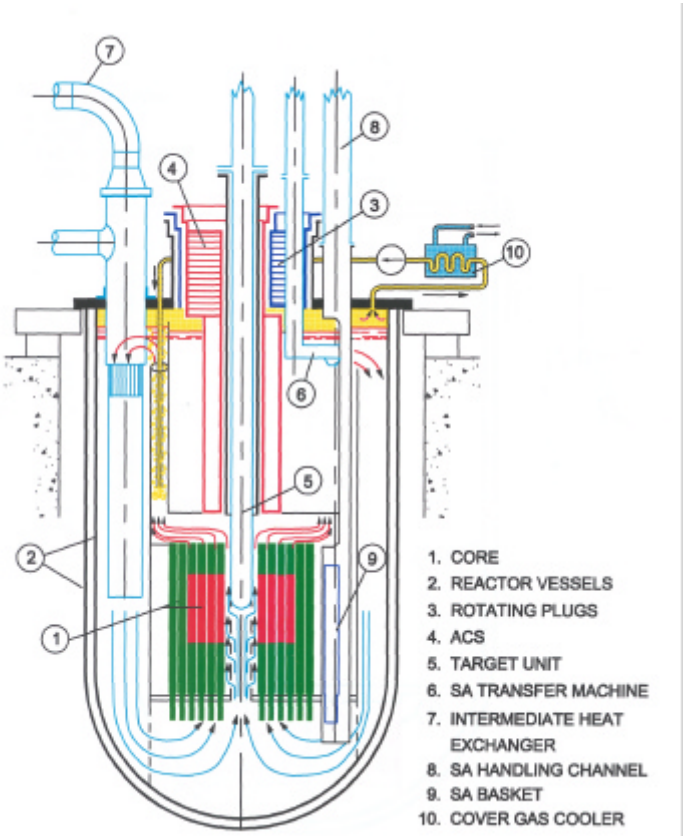

Figure 5-5. Ansaldo's preconceptual design of a demonstration facility of an ADS.

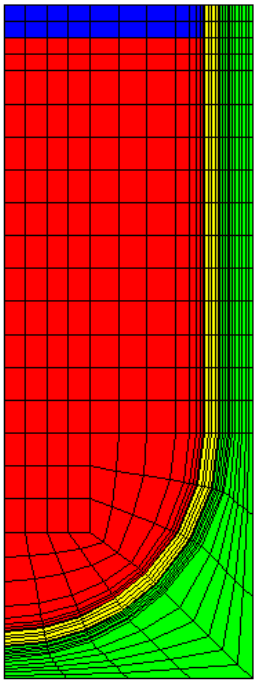

- Red color represents the Pb/Bi coolant

Blue color represents the argon filled gas plenum

Yellow color represents the gap between the reactor and guard vessel, which is filled with air

Green color represents the RVACS air circuit (downcomer

Figure 5-6. The computational mesh used in the calculations.

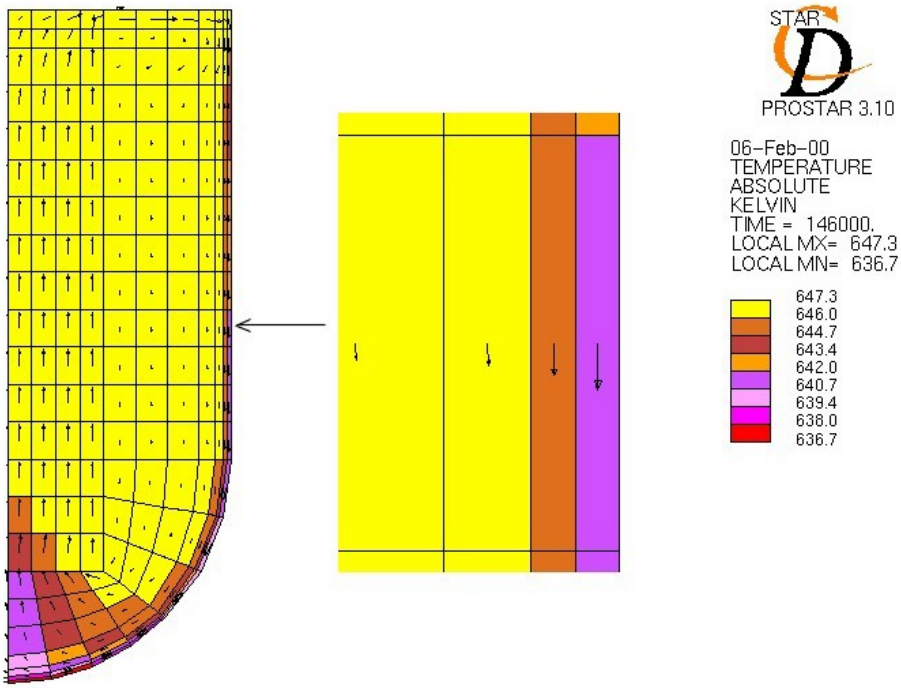

*Figure 5-7. Example of coolant temperature and velocities in the reactor vessel of the **modified** Ansaldo design (power of 800MWth) for LOHS accident with gap filled and water spray cooling. The detail shows that the Pb/Bi is preferably running down close to the vessel wall, the velocities being higher due to lower temperatures and thereby higher densities.*

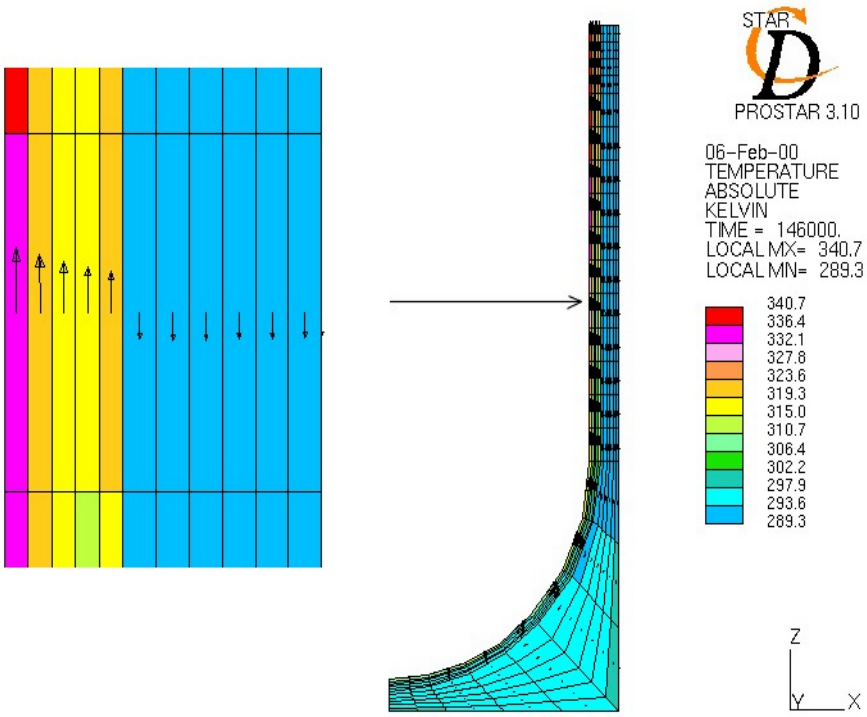

*Figure 5-8. The coolant velocities and temperatures in the riser and downcomer of the RVACS air channel of the **modified** Ansaldo design (800MWth) for LOHS accident with gap filled and water spray cooling.*

The RVACS air channel surrounds the guard vessel with a gap width of 18 cm. It is separated from an air downcomer by a thermally insulated collector wall.

The computation was performed on the mesh seen in Fig 5-6. Figures 5-7 and 5-8 exemplify the temperatures and velocities at the end of the calculation, i.e. at 40 hours for the design of 800 MWth.

5.3.2 Computational set-up and physical properties

In the reference calculations, it was assumed that an RVACS relies only on air-cooling and no additional cooling means are employed. All walls were treated as hydrodynamically smooth, meaning that the roughness is such that the boundary layer next to the surface has a practically undisturbed profile. The emissivity is set to 0.75, which is appropriate for steels with a heavily oxidised surface [37]. Neither fins, nor other heat transfer improving devices are used.

The core has been modelled as a porous medium, where the power generation is distributed uniformly. The pressure drop over the core is 20kPa at 0.42m/s; thereafter the pressure drop is linearly proportional to the velocity. Similarly, the pressure drop in the rest of the reactor vessel, including the heat exchangers, is 9kPa at 0.42m/s [31].

The heat transfer correlation used on the airside was developed at ANL, see Eq. 2. A correlation for liquid metals is used for calculating the heat transfer coefficient reactor

vessel on the Pb/Bi coolant side. The correlation is derived from the theory of the relation between the temperature and velocity profiles in liquid metals [34].

The decay heat generation immediately after beam-stop has been preliminary based on experimental data from a PWR [28]. Within less than 10 seconds, the power generation drops to about 6.7% of the normal operation power, i.e. 5.3 MWth for the 80MWth ADS. Thereafter, the power generation is modelled as a function of time according to Fig. 5-9. For the purpose of these calculations an assumption has been done, that for the

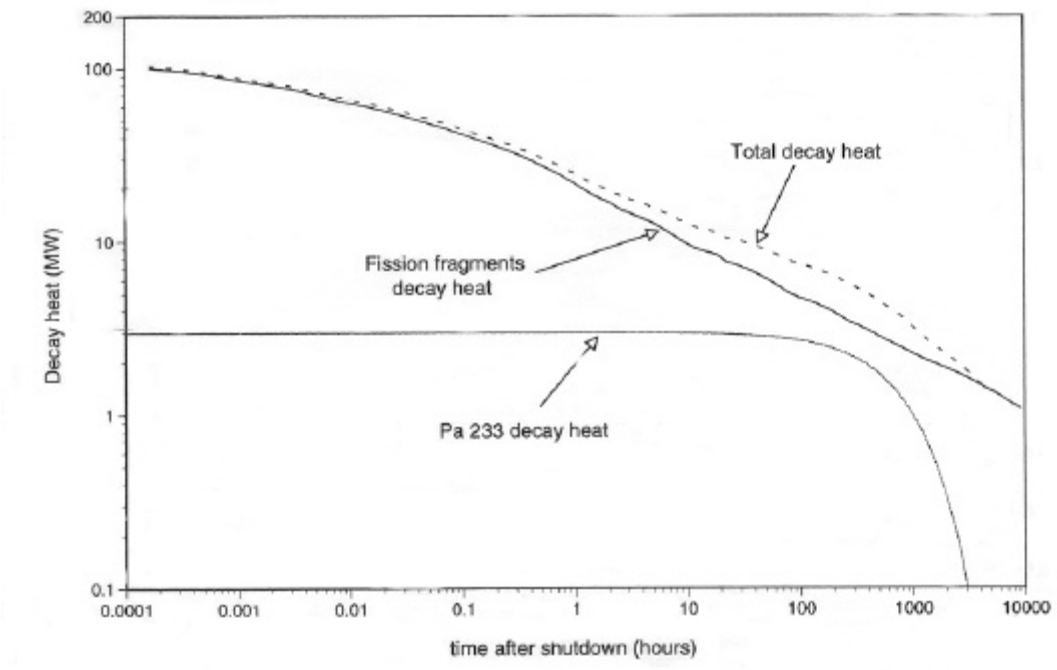

Figure 5-9. The decay heat generation for a 1500MWth ADS reactor as a function of time [28] .

time intervals relevant for these studies, there are no significant differences in decay heat generation between an ADS fuelled with U-Pu and Th-U, and that decay heat curves can be rescaled for different power levels.

5.4 REACTOR VESSEL AUXILIARY COOLING SYSTEM OF AN 80MW$_{th}$ ADS REACTOR

5.4.1 Temperature in reactor coolant as a function of time after normal beam-stop

This scenario investigates a simultaneous LOHS and LOF accident. It is assumed that the failure is detected and the proton beam shut off within 10 seconds. In a station blackout accident the beam would actually be switched off at the same time as the pumps. Thus, the calculational results for a station blackout are slightly conservative. The fact that forced convection is not functioning, means that no Argon bubbles are injected above the core any longer and thus the effect of greater density difference in the riser and downcomer vanishes. The static pressure difference between the riser and the

downcomer is thus reduced. The density effect from the remaining bubbles in the riser has disappeared after 10 seconds and the flow speed is almost halved.

In this case the average temperature above the core reaches its maximum after 10 hours at about 654K. With a core of pitch-to-diameter (P/D) ratio of ~1.9, the surface cladding temperature reaches about 20K more, i.e. 673K. This temperature is well below acceptable limits, the cladding corrosion process increases above 893K when the protecting oxide layer becomes unstable [41]. The maximum Pb/Bi coolant velocity has to be limited to maximum 3m/s to avoid rupturing the protective oxide layer [39].

The highest reactor vessel wall temperatures are expected at the top of the reactor, due to the fact that the hot coolant hits the wall at this location first. They are only a few degrees K lower than the coolant temperatures show. Hereafter, the coolant will flow in the downward direction. Directly adjacent to the wall it has the highest downward velocity of about 0.12m/s. This relatively high velocity compared to the rest of the downcomer is a consequence of the increasing density of the cooled Pb/Bi. The wall surface above the heat exchanger reaches of 631K after 10 hours, which is about 20K lower than above the core.

The temperatures on the airside reaches about 373K next to the guard vessel wall, and the temperature next to collector wall about 343K. The elevated temperatures next to the collector wall are mainly due to heat transfer by thermal radiation. The velocities in the air channel reach 2.7m/s at the most.

5.4.2 Temperature in reactor coolant as a function of time after delayed beam-stop

This calculation also assumes a LOHS and LOF accident event. Moreover, the proton beam is operating another 30 minutes after the accident initiation, i.e. the reactor power remains at 80MWth. It can be noted that this situation is a highly unlikely since in the case of a station blackout the accelerator would loose power too. If this state persists during the 30 minutes, the temperature increases to 1346K above the core in the reactor vessel. The 30 minutes were selected since this is the time during which every

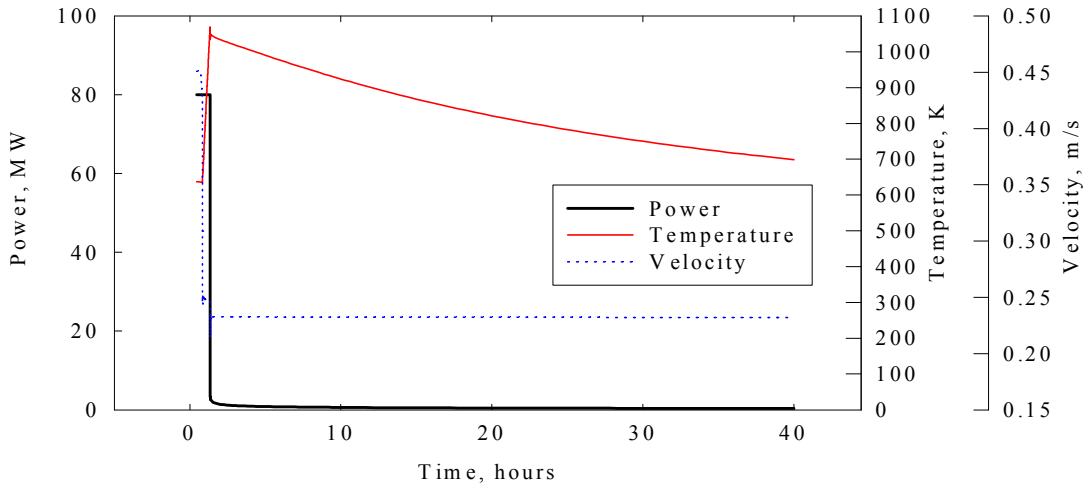

Figure 5-10. The coolant temperature and velocity development above the core in a 80MWth ADS reactor. The beam shut-off is delayed 30 minutes.

counteraction should be automated in Swedish NPP, which allows the operators to consider what further action to carry out meanwhile [40]. After beam shut-off, the temperature profile is similar to the previous case, the main difference is a shift towards higher temperatures in the coolant. The heat removal works better due to the higher guard vessel temperature, which gives the curve a flatter profile, see Fig. 5-10.

5.5 LOSS-OF-HEAT SINK AND LOSS-OF-FLOW CALCULATIONS BASED ON AN 800MW$_{th}$ ADS REACTOR

5.5.1 Temperature in reactor coolant as a function of time after normal beam-stop

Investigations of the heat removal from an ADS reactor with ten times the power of the demo design (800 MW$_{th}$) have been performed. This investigation is motivated by the notion that future ADS plants will have a higher power to vessel surface area ratio than the 80MWth reactor. The dimensions of the whole plant were kept as in the 80MW$_{th}$ investigations for reasons of comparison. It should be noted that the dimensions of the reactor vessel would probably be larger for a more realistic 800MWth design. Therefore our results are conservative, but an indication of the RVACS efficiency for higher power systems. It should also be mentioned that no attempt was yet made to increase the RVACS efficiency by including fins and/or enhancing the surface emissivity.

As in the investigation of the 80MW$_{th}$ plant, the beam is shut off 10 seconds after the LOF and LOHS accident. Due to the higher power to vessel surface ratio compared to the 80MWth reactor, the coolant maximum temperature is not reached until 23 hours at 1338K. This temperature will cause vessel creep. The latter starts above 1173K for long time (hours) at these temperatures [38]. Figure 5-11 displays the coolant temperature variation with time.

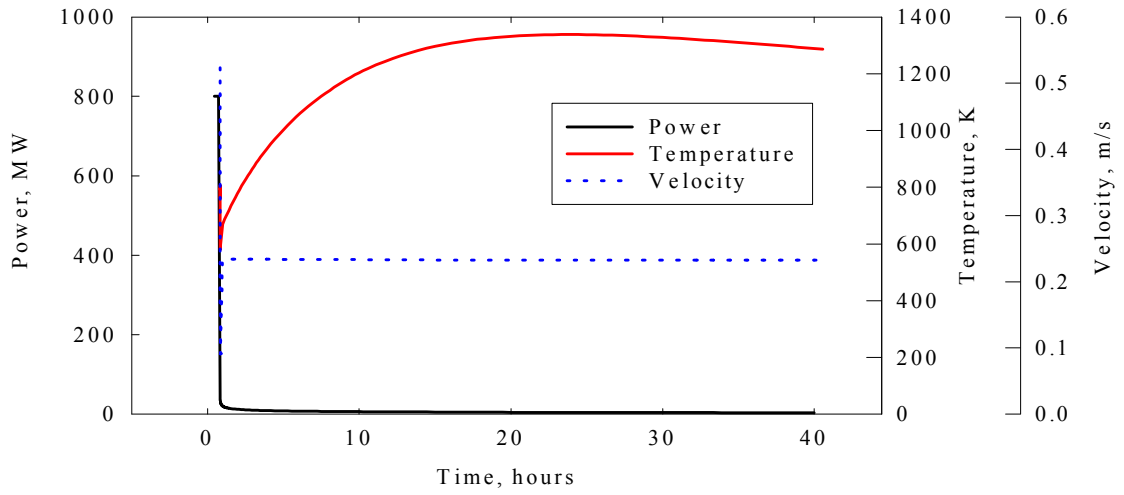

Figure 5-11. The coolant temperature and velocity development above the core in an 800MWth ADS reactor. Beam is shut off immediately

5.5.2 Temperature in reactor coolant as a function of time after normal beam stop with additional spray cooling applied

To decrease the coolant temperatures in LOHS events, water spray cooling on the outside of the guard vessel can be applied [30]. The evaporation process of the water droplets requires a lot of energy, and can thereby be an excellent complement to the normal air-cooling at times when more effective heat removal is required. On larger reactor types, the spray cooling would be even more useful, since conventional RVACS becomes less effective the larger the reactor size due to the fact that the ratio between the power produced and the outside area of the guard vessel becomes greater.

In this examination, the heat removal from spray cooling is calculated analytically [33]. The droplet size was chosen as 2mm diameter and the flow rate 100kg/s, at which the heat transfer efficiency is 0.10 above 500K. The heat transfer efficiency is a function of the total energy needed to heat and evaporate a droplet. As a conservative approach, the heat transfer efficiency is assumed to decay linearly to zero between 500K to 373K. The calculated heat removal is then subtracted from the surface of the guard vessel wall as a function of temperature. The temperature and velocity above the core can be seen in Fig. 5-12.

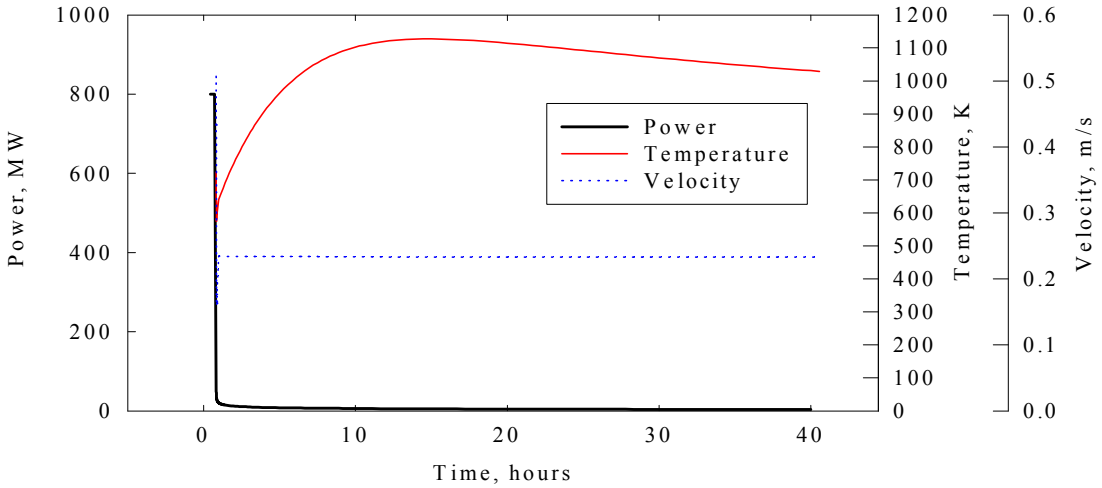

Figure 5-12. The coolant temperature and velocity development above the core in an 800MWth ADS reactor. The beam is shut off immediately and water spray cooling applied

The spray cooling is started about 10 seconds after the LOHS initiation. This more efficient cooling has the effect of that the heat removal is exceeding the decay heat generation earlier after shutdown and lower maximum temperatures are reached. Consequently, the maximum temperature peaks at about 14 hours instead of 25 hours after shutdown, as was the case with air-cooling. The maximum temperature is also reduced to about 1130K, or about 200K lower than in the pure air-cooling RVACS. The gap between the reactor and guard vessel acts as an insulating space with a large temperature gradient; i.e. the guard vessel has very low temperatures whereas the reactor vessel remains on relatively high temperatures. This causes a reduction of the decay heat removal efficiency. The temperature of 1130K is acceptable for the structural materials. However, the cladding will be damaged if the high temperatures

remain for too long [41]. Figure 5-12 displays the temperature and velocity development in coolant above the core.

5.5.3 Temperature in the reactor coolant as a function of time after normal beam-stop with filled gap

Another measure to increase the heat removal is to fill the gap between the reactor and the guard vessel [28]. The gap can be filled with for instance the Pb/Bi coolant, which is highly conductive compared to air. The heat will be transferred to the guard vessel more efficiently, and consequently reaches higher temperatures. Accordingly, the air temperatures and the heat removal rate also increase. The maximum coolant temperature of 1273K is reached in the reactor vessel, only 65K lower than the reference case with air-cooling. The temperature and velocity can be seen as a function of time in Fig. 5-13.

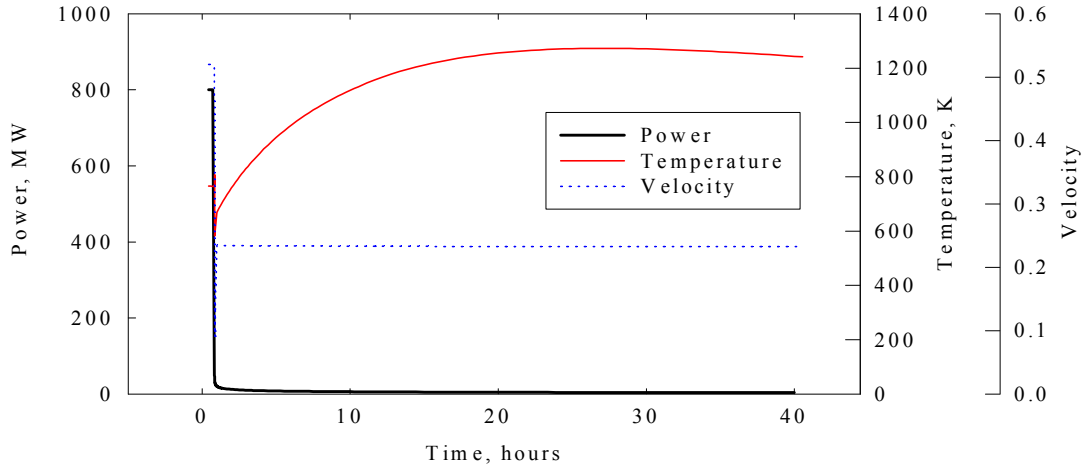

Figure 5-13 The coolant temperature and velocity development above the core in an 800MWth ADS reactor. The beam is shut off immediately and the gap between the reactor and guard vessel is filled.

5.5.4 Temperature in the reactor coolant as a function of time after normal beam-stop with both the gap filled and spray cooling activated

In this case both the gap between the reactor and guard vessel was filled with Pb/Bi coolant, and the water spray cooling was utilised concurrently. Thus, good heat conduction between the reactor and guard vessel was achieved, at the same time as extra heat removal through the evaporation of droplets was activated.

As can be seen in Fig. 5-14, the decay heat removal is exceeding the decay heat generation already 2 minutes after the LOHS initiation. The maximum coolant temperature peaks at 780K. The heat removal is very efficient and an 800MWth ADS plant can easily be cooled if the proton beam is shut off immediately.

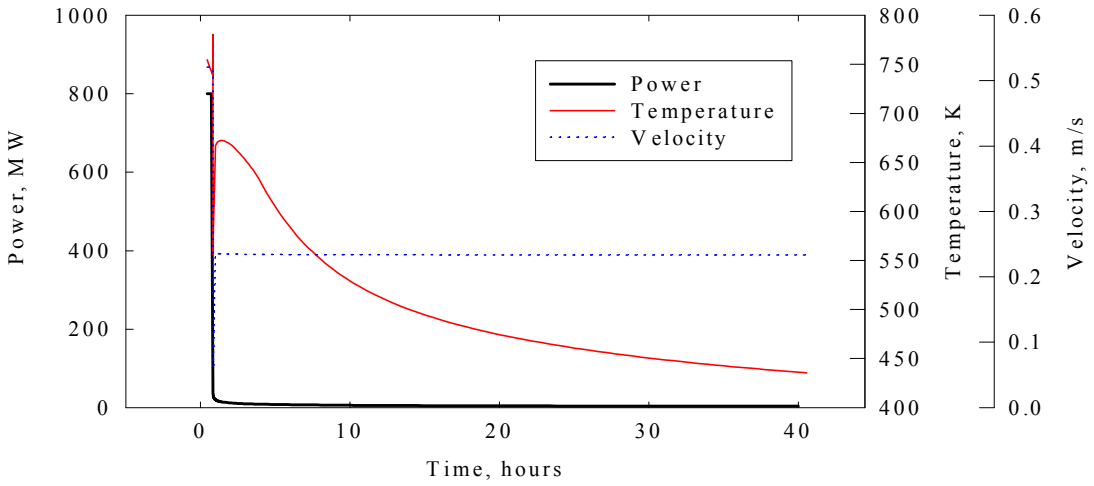

Figure 5-14. The coolant temperature and velocity development above the core in an 800MWth ADS reactor. The beam is shut off immediately, the gap between the reactor and guard vessel is filled, and water spray cooling is applied

5.5.5 Temperature in reactor coolant as a function of time after delayed beam-stop

During an LOHS the accelerator proton beam can only be left on for a limited period of time before shut-off is necessary so that structural material problems with the reactor vessel are avoided. In this calculation the gap is to be filled when the temperature in the reactor vessel wall exceeds 1023K, and the spray cooling starts when the guard vessel temperature is higher than 500K.

The additional heat removal improving measures, i.e. filled gap and spray cooling are not making a major difference as long as the beam is operating. But, as soon as the accelerator is switched off they can reduce the time after beam-stop when the coolant temperature peaks. With filled gap and the spray cooling applied, the temperature will reach 1504K after the five initial minutes while the beam is still on. At beam stop, the power generation is about 6.7% [28] of normal operating power whereas the flow velocity is maintained longer due to its inertia. Thus the temperature above the core is reduced 214K in half a minute to 1290K. Thereafter, the temperature increases again until the decay heat removal is greater than the decay heat generation. The second maximum temperature is reached at 1388K, 25 minutes after beam-stop, see Fig. 5-15. The maximum coolant temperature is below 1200K after about five hours.

The reactor vessel will melt at about 1700K, and it should not be exposed to temperatures above 1200K for longer periods due to structural creep of the vessel, i.e. hours [38]. A five minutes beam-stop delay is hence about as much as the reactor vessel can cope with.

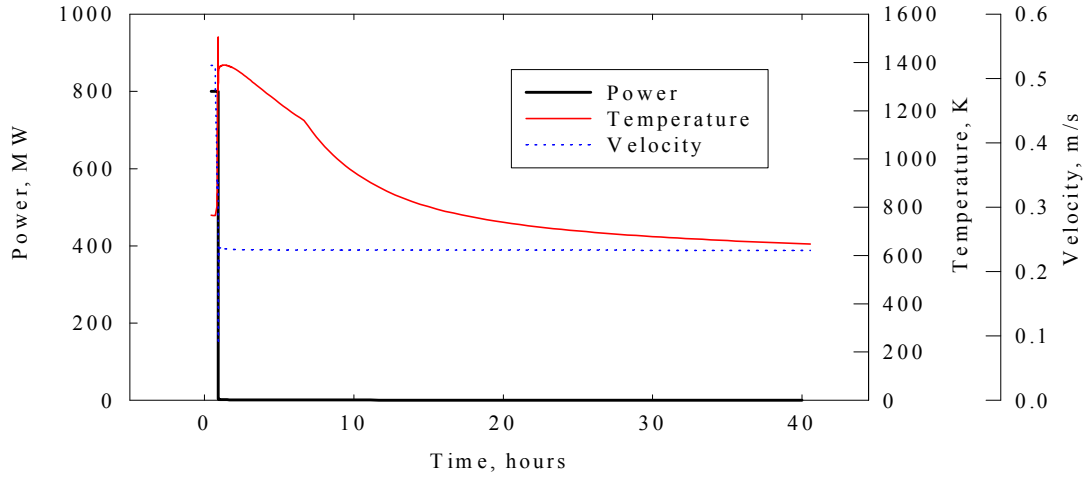

Figure 5-15. The coolant temperature and velocity development above the core in an 800MWth ADS reactor. The beam shut-off is delayed 5 minutes, the gap between the reactor and guard vessel is filled, and water spray cooling is applied.

5.6 CONCLUSIONS ON LOHS CALCULATIONS FOR LARGER AND SMALLER ADS THERMAL POWERS AND ON A LATE SWITCHING OFF OF THE PROTON BEAM

The calculations on the 80 MWth Ansaldo ADS show that an RVACS with air-cooling is an attractive approach for lower power systems. Although the calculations for the higher power ADS are very conservative because the relatively small vessel of the Ansaldo design was used, they show a clearly lower performance for larger systems. New approaches may be needed. It was demonstrated that water spray cooling of the guard vessel outside together with the filling of the gap between the reactor and the guard vessel with liquid Pb/Bi leads to a very efficient heat removal. However, even with the considerably larger heat removal capacity, only an increase in the grace time can be achieved in the highly unlikely case of an LOHS together with a late switching off of the proton beam. A long-term removal of the full ADS power by ex-vessel cooling does not appear possible.

6 NEUTRON AND PROTON CROSS-SECTION EVALUATIONS FOR ^{232}Th, ^{238}U AND ^{239}Pu FOR ENERGY RANGE UP TO 150 MeV

In collaboration with a Russian group from the Institute of Physics and Power Engineering (IPPE) in Obninsk and partially in the frame of European Project "IABAT" [43] neutron and proton cross section evaluations have been performed for ^{232}Th, ^{238}U and ^{239}Pu as a part of broader international activities of building up intermediate energy nuclear data libraries.

The starting point of serious computational modeling of a realistic accelerator-driven system is basic nuclear reaction information. There are basically two ways to provide a link between thin target nuclear reaction measurements and applied analyses. The first method, which is traditionally linked with high energies, is to perform the calculation of both microscopic nuclear reactions and macroscopic transport processes by the same computer code. HETC, LAHET and FLUKA [44] are well-known examples of intranuclear cascade codes that work according to this principle. Quality statements about such codes can be obtained by comparison of the results with available thin-target experimental data. Then, after choosing geometry specifications for the accelerator, target and/or the reactor, the code could be set in "production mode" to predict processes that take place in a realistic device. Additional validation is possible using integral experiments, in which the neutron flux and other macroscopic quantities of interest can be measured for a thick target.

The alternative method, nuclear data evaluation, is more modular, not only in a computational sense but also from the point of view of human expertise. It is based on the benchmarking of one or more designated scattering and reaction model codes against available experimental data and subsequent storage of the calculated data into evaluated data files [45] [46] in a well-defined manner: the Evaluated Nuclear Data Format version 6, in short the ENDF6-format [47]. Whenever measurements are too difficult to predict, e.g. in the case of residual production cross-sections, one can also directly include experimental data in the data file. Hence, since one is in the position to use the best available code or experimental data for each partial nuclear reaction channel, as long as certain sum rules are obeyed, the data evaluation method arguably allows the closest possible connection between nuclear reaction physics and practical applications. After processing, the data libraries can serve as input for deterministic or Monte-Carlo nuclear transport codes. For a few decades evaluated data files have served as crucial ingredients of fission and fusion reactor research. The same situation is ahead of us for ADS.

At present, the intranuclear cascade and data evaluation methods are regarded as complementary valuable approaches for analyses of accelerator-driven systems. The many years effort in fission and fusion reactor studies has resulted in well-benchmarked data files that cover nuclear reactions up to ~20 MeV. However, the matching energy between the two methods should be around 150 MeV. There are several reasons for this particular energy and a detailed explanation of these reasons would fall beyond the scope of this report. It is however important to note that for radiation damage assessment, shielding calculations and most probably for predictions of the fuel

behaviour in ADS, data libraries may prove to be important when eventually nuclear industry desires engineering data for accelerator-driven systems.

There are several reasons to limit nuclear data libraries at energy of 150 MeV:

- above 150-200 MeV, pion production becomes important and the present low-energy codes (and the ENDF6-format) do not yet cover such reactions;
- above about 150 MeV new physics for reliable optical model parameterizations that should have predictive power in regions where there is no experimental data is required;
- the deterministic nuclear model codes that are successfully used up 150-200 MeV cannot handle more than two fast particles in the outgoing channel;
- the present transport codes have not yet the capability to properly transport charged particles.

6.1 METHODOLOGY OF NEUTRON DATA EVALUATIONS

For the incident neutron energy below 20 MeV the evaluations of ENDF/B-VI, BROND-2 [48] and JENDL-3.2 were used as a rule with an addition of ENDF/B-VI evaluations for the fast neutron inelastic scattering cross sections. The discrepancies between various evaluations are significant but nowadays there are not enough experimental data to improve available evaluations.

Evaluations above 20 MeV have been based on nuclear model calculations fitted to experimental data where available. The coupled-channel optical model has been used to calculate the neutron transmission coefficients and to evaluate the neutron elastic scattering angular distributions [49]. The GNASH code [50] was used to calculate the integral and double differential cross sections and to prepare data into the ENDF/B-VI format. The level density description for all channels was obtained on the basis of the Gilbert-Cameron approach fitted to experimental data on the density of low-lying levels and neutron resonances [51]. Neutron and proton transmission coefficients were obtained from the optical potentials [49], as discussed below. Transmission coefficients for alpha, deuterons and tritons were calculated using spherical optical model.

6.2 TOTAL AND SCATTERING NEUTRON AND PROTON CROSS SECTIONS

Evaluations of neutron total cross sections have been based on the coupled-channels optical model calculations with potential parameters fitted to experimental data. This procedure gives satisfying results for the total neutron cross sections. However, the calculated neutron absorption cross sections show significant discrepancies for various data libraries. These discrepancies are essential at neutron energies above 10 MeV, and their effects appear in the evaluated cross sections of (n,xn), fission and other reactions.

The optimal set of optical model parameters has been estimated from the analysis of experimental data of neutron total cross sections, angular distributions for proton elastic scattering and proton absorption cross sections. These parameters, shown for ^{232}Th, ^{238}U and ^{239}Pu in Tables 6-1, 6-2 and 6-3, respectively, are close to those used for the intermediate energy neutron cross section evaluations of lead isotopes [52] [53] .

Table 6-1: ^{232}Th optical potential parameters for neutrons and protons.

Well depth (MeV)	Energy Range (MeV)	Geometry (fm)
$V_R = 53.425 \pm 16\eta - 0.279E + \Delta_C$	$0 < E < 60$	$r_R = 1.183$; $a_R = 0.797$
$V_R = 114.447 \pm 16\eta - 19 \ln(E) + 2.$	$60 < E < 200$	
$W_d = 2.694 \pm 8\eta + 0.252E$	$0 < E < 14$	$r_d = 1.273$; $a_d = 0.699$
$W_d = 6.222 \pm 8\eta - 0.0932(E-14.)$	$14 < E < 200$	
$W_V = 0.0$	$0 < E < 14.4$	$r_c = 1.26$
$W_V = -2.6 + 0.18E$	$14.4 < E < 40$	$r_V = 1.373$; $a_V = 0.699$
$W_V = 2.2 + 0.06E$	$40 < E < 100$	
$W_V = 8..2 + 0.018(E-100.)$	$100 < E < 200$	
$V_{SO} = 6.18$	$0 < E < 200$	$r_{SO} = 1.16$; $a_{SO} = 0.667$

Here $\eta = (A-2Z)/A$; $\beta_2 = 0.19$, $\beta_4 = 0.071$ and the scheme of $0^+ - 2^+ - 4^+ - 6^+$ coupled levels is adopted.

Table 6-2: ^{238}U optical potential parameters for neutrons and protons.

Well depth, MeV	Energy Range, MeV	Geometry, fm
$V_r = 52.33 \pm 16\eta + 0.04306E - 0.02377E^2 + \Delta_c$	$0 < E < 14$	
$V_r = 51.192 \pm 16\eta - 0.2085E + \Delta_c$	$14 < E < 65$	$r_v = 1.185$, $a_v = 0.8$
$V_r = 53.096 \pm 16\eta - 0.2377E + \Delta_c$	$65 < E < 150$	
$\Delta_c = 0.4Z/A^{1/3}$		$r_{coul} = 1.26$
$W_d = 3.082 \pm 8\eta + 0.8477E - 0.01924E^2$	$0 < E < 10$	
$W_d = 11.1232 \pm 8\eta - 0.14882E$	$10 < E < 50$	$r_d = 1.26$, $a_d = 0.52$
$W_d = 8.067 \pm 8\eta - 0.08235E$	$50 < E < 150$	
$W_V = 0.0$	$0 < E < 14.4$	
$W_v = -1.7843 + 0.12745E$	$14.4 < E < 65$	$r_v = 1.26$, $a_v = 0.5 + 0.0125E$
$W_v = 2.9792 + 0.05417E$	$65 < E < 150$	
$V_{so} = 6.18$	$0 < E < 150$	$r_{so} = 1.16$, $a_{so} = 0.667$

Here $\eta = (A-2Z)/A$; $\beta_2 = 0.23$, $\beta_4 = 0.045$ and the scheme of 0^+-2^+-4^+-6^+coupled levels is adopted.

Table 6-3: ^{239}Pu optical potential parameters for neutrons and protons.

Well depth, MeV	Energy Range, MeV	Geometry, fm
V_r=51.50 ±16η+0.2420E + Δ_c	0 < E < 40	
V_r = 50.58 ± 16η - 0.2190E + Δ_c	40< E < 100	r_v = 1.21, a_v = 0.7
V_r = 49.34 ± 16η - 0.2066E + Δ_c	100< E < 150	
Δ_c = 0.4Z/$A^{1/3}$		r_{coul} = 1.26
W_d = 3.36 ± 5η + 0.4691E -	0 < E < 5.24	
W_d = 2.079 ± 5η + 0.14882E - 0.0212E^2	5.24 < E < 22	r_d = 1.32-0.0055E, a_d =.63
W_d = 8.067 ± 5η - 0.08235E	22 < E < 35	r_d = 1.2, a_d=0.47-0.008E
W_d = 9.053 ± 5η - 0.0867E	35<E<100	r_d = 1.2, a_d=0.75
W_d = 1.523 ± 5η - 0.01147E	100<E<150	
W_V = -1.708 + 0.122E - 0.000022E^2	0 < E < 100	r_v = 1.26, a_v = 0.35+0.0018E
W_v = -0.408 + 0.107E - 0.0002E^2	100< E < 150	
V_{so} = 6.18	0 < E <150	r_{so} = 1.16, a_{so}=0.667

*Here η = (A-2Z)/A; β_2 = 0.205, β_4 = 0.075 and the scheme of $1/2^+$-$3/2^+$-$5/2^+$-$7/2^+$-$9/2^+$ coupled levels is adopted.

The total cross sections calculated with the parameters given above are compared in Figs 6-1, 6-2, 6-3 with available experimental data and other calculations. Below 20 MeV there are many experimental data and only some of them are presented. A reasonable agreement of our evaluation with the Barashenkov's systematics [54] and experimental data is obtained for all energies above 20 MeV.

An example of neutron elastic scattering and absorption cross-sections for ^{239}Pu is shown in Figs 6-4 and 6-5, respectively. There are no direct measurements of these cross sections at high energies. However, a reasonable estimation of them is given by Barashenkov's systematics, based mainly on proton reaction data [54]. The optical model calculations reproduce well the proton absorption cross section in the whole energy region from the Coulomb barrier to 200 MeV, and at high energies they are in reasonable agreement with the Barashenkov evaluations for both protons and neutrons.

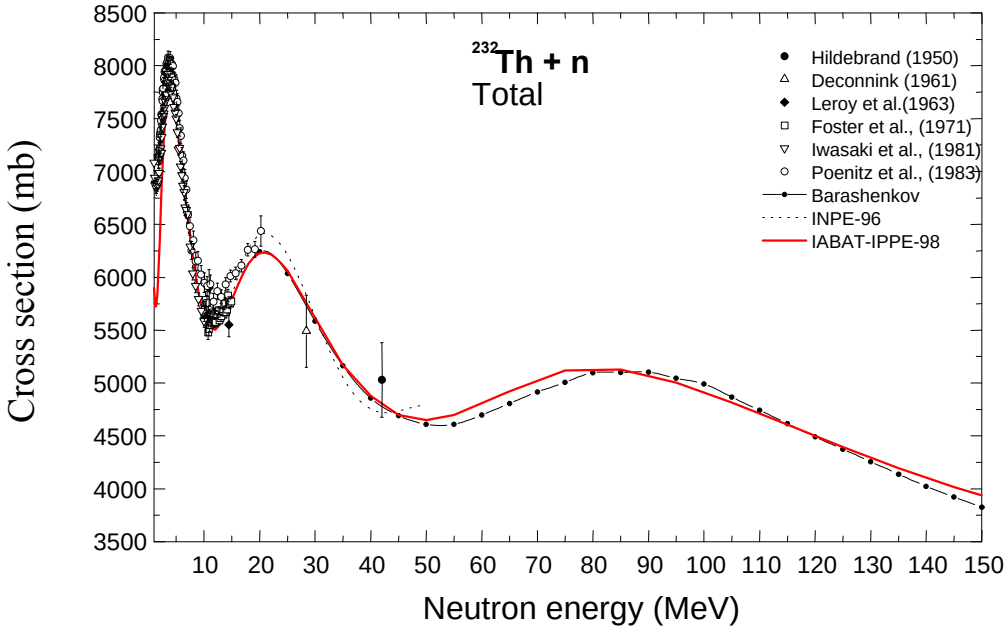

Figure 6-1. Comparison of different calculations of the ^{232}Th total neutron cross section with experimental data and other evaluations.

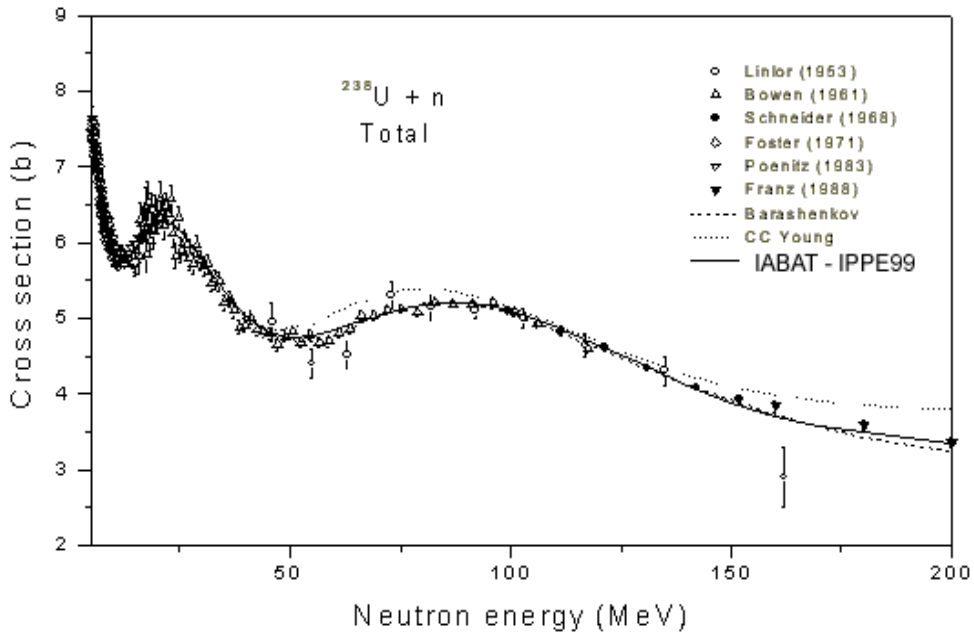

Figure 6-2. Comparison of different evaluations of the ^{238}U total neutron cross section with experimental data.

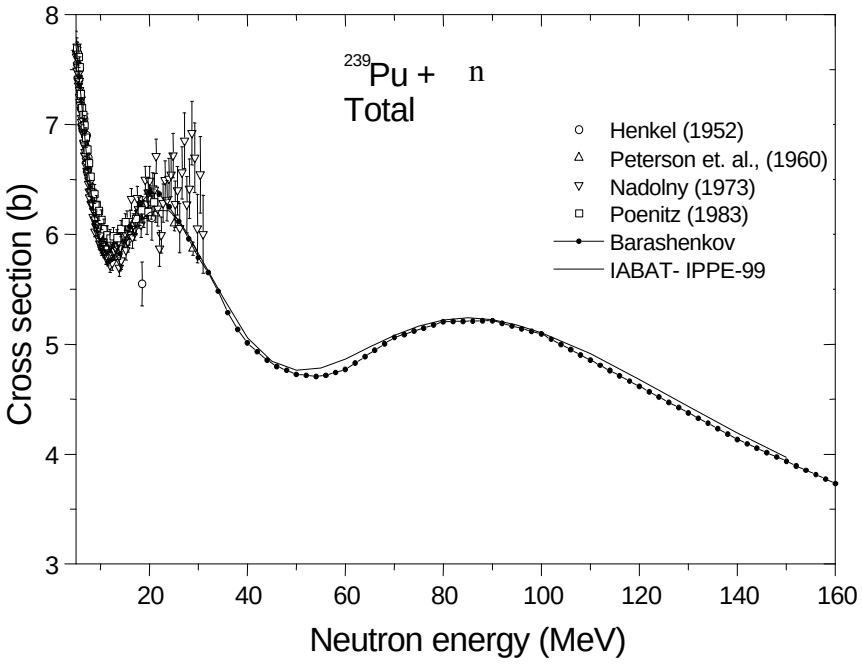

Figure 6-3. Comparison of different evaluations of the ^{239}Pu total neutron cross section with experimental data.

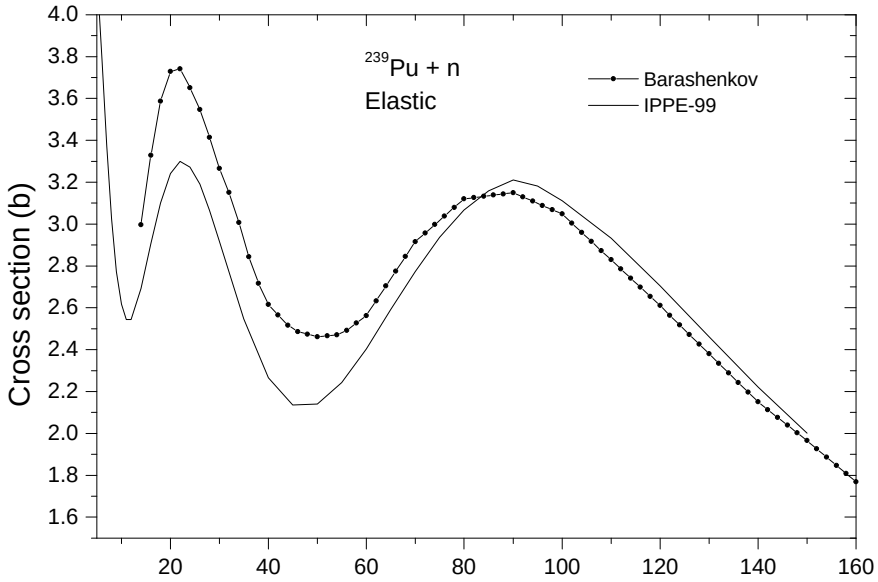

Figure 6-4. Comparison of Barashenkov's systematics and evaluation of the elastic neutron cross section for ^{239}Pu.

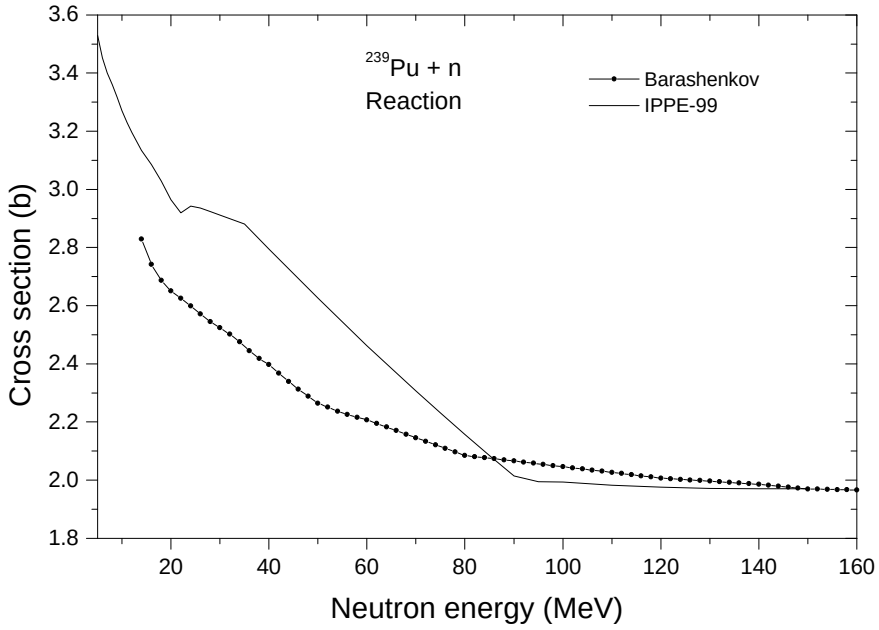

Figure 6-5. Comparison of evaluated neutron capture reaction cross section and systematics for ^{239}Pu.

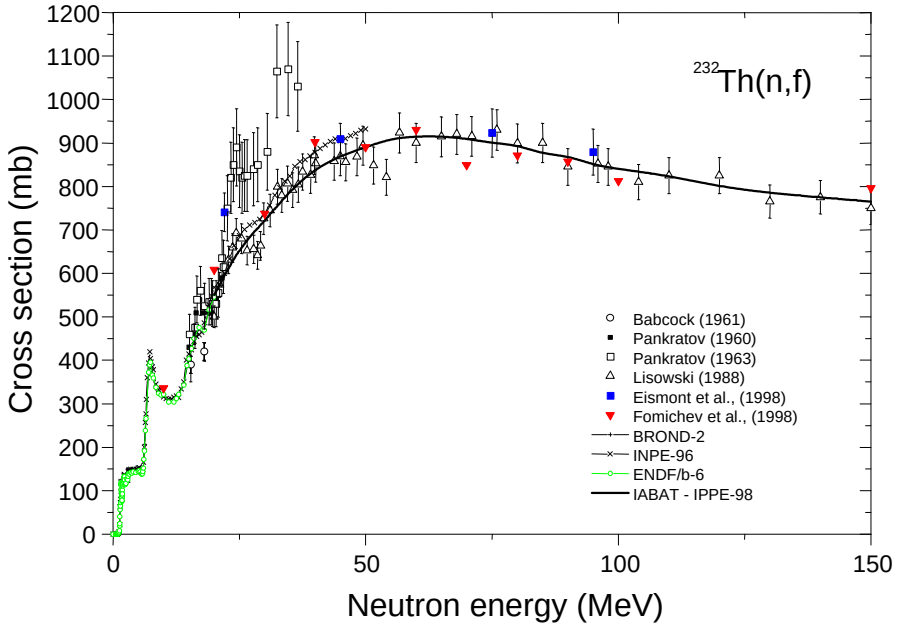

Figure 6-6. Comparison of the evaluated fission cross section for ^{232}Th with experimental data and previous evaluations.

6.3 FISSION CROSS SECTIONS AND FISSION PROMPT NEUTRONS

The fission cross section of ^{232}Th, ^{238}U and ^{238}Pu for neutrons and protons with energies above 20 MeV was measured by several research groups and comparisons between different experiments and evaluation data are presented in Figs 6-6, 6-7 and 6-8. Except for some large discrepancies for ^{232}Th [55] and ^{239}Pu [56] older experimental data in the energy range 25 – 50 MeV, the evaluated data fits well into experiments.

For low energy range, up to 20 MeV, the evaluated fission cross sections were fitted to the ENDF/B-VI data in order to obtain fission barrier parameters. For higher energies, the effects of nuclear viscosity were included in the calculations of the fission widths of highly excited compound nuclei [57]. An accurate description of the fission cross sections is very important for consistent evaluation of multiple emission of neutrons and charged particles.

The result of evaluation for <ν>, the average number of prompt neutrons per fission, is shown in Fig. 6-9 for ^{232}Th, ^{238}U, ^{239}Pu, in the energy range up to 150 MeV. Scarce, existing experimental data of Fréhaut [58] and of Korovin [59] are also plotted on these figures.

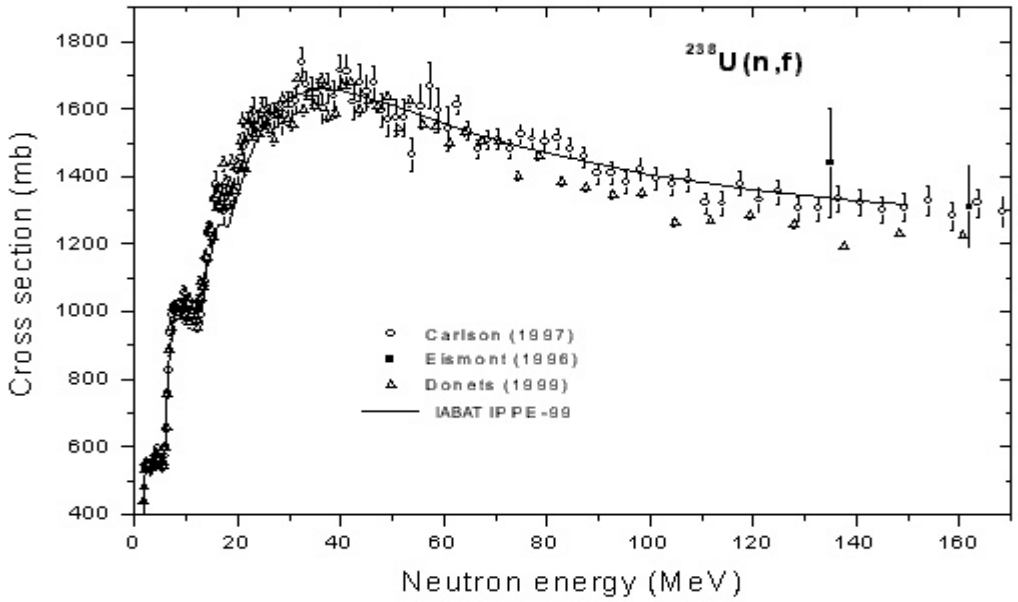

Figure 6-7. Comparison of the evaluated fission cross section for ^{238}U with experin

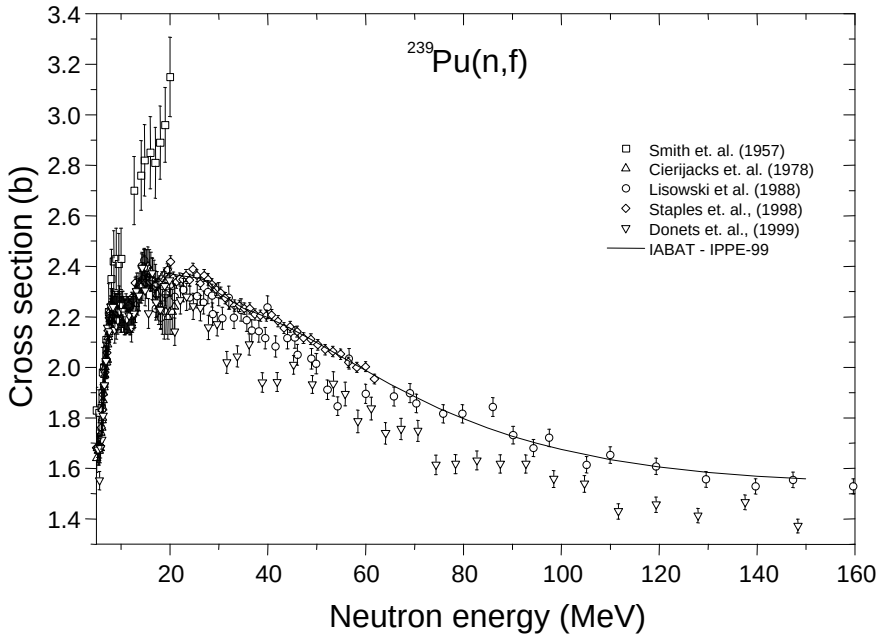

Figure 6-8. Evaluated and experimental fission cross section for ^{239}Pu.

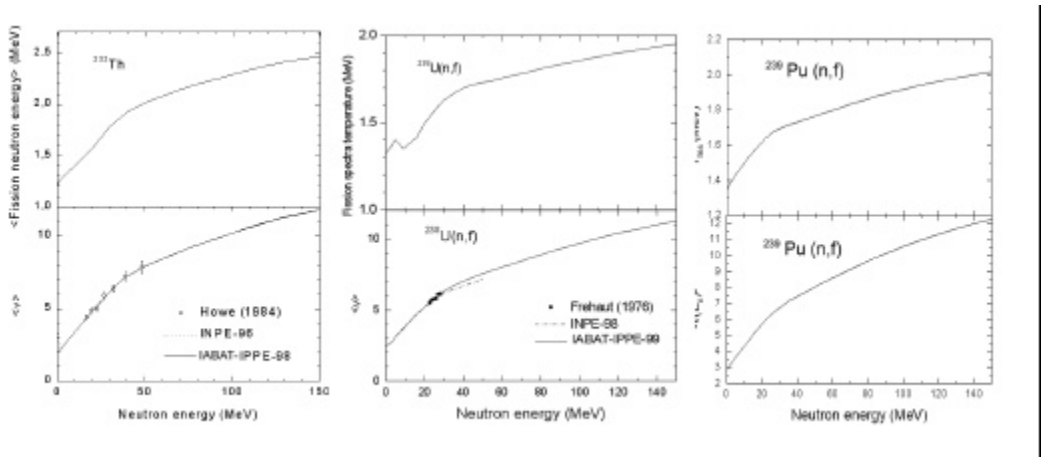

Figure 6-9. Average fission neutron energy and number of neutrons <n> for ^{232}Th, ^{238}U and ^{239}Pu as a function of neutron energy.

6.4 NEUTRON PRODUCTION CROSS SECTIONS AND SPECTRA

Evaluations of particle emission spectra and corresponding production cross sections have been performed in accordance with the rules of the ENDF/B-VI format for the double-differential cross sections, by using the Kalbach-Mann representation of such data [60]. Differential cross sections are described in this approach by the integral production cross section for the corresponding emitted particle multiplied by a normalized angular distribution function of the following form,

$$f(m_b, E_a, E_b) = f_0(E_a, E_b)\left\{\frac{a(E_a, E_b)}{\sinh a(E_a, E_b)}\left[\cosh\left(a(E_a, E_b)m_b\right) + r(E_a, E_b)\sinh\left(a(E_a, E_b)m_b\right)\right]\right\}$$

where E_a is the incident particle energy in the laboratory system, μ_b is the scattering angle cosine of the emitted particle b and E_b is its energy in the center-of-mass system, $f_0(E_a,E_b)$ is the normalized spectrum of the emitted particle, $r(E_a,E_b)$ is the pre-compound fraction of this spectrum, and $a(E_a,E_b)$ is the simple function proposed in [60], which depends mainly on the center-of-mass emission energy E_b and, to a lesser extent, on particle type and incident energy at higher values of E^a . In accordance with such a description, the two energy-dependent functions $f_0(E_a,E_b)$ and $r(E_a,E_b)$ determine completely the shape of emitted particle spectra and the anisotropy of the corresponding angular distributions, respectively.

The neutron emission is a dominant reaction that competes with nuclear fission. The example of neutron production cross-section for ^{238}U is shown in Fig. 6-10. Below 20 MeV these calculations agree well enough with the evaluations of the (n,2n) and (n,3n) reactions based on experimental data and included in the files of BROND-2 or ENDF/B-VI. Above 20 MeV, there are no direct experimental data on neutron emission cross sections or on the multiplicity of secondary neutrons, which can be evaluated as the ratio of the calculated neutron production cross section to the reaction cross section considered above.

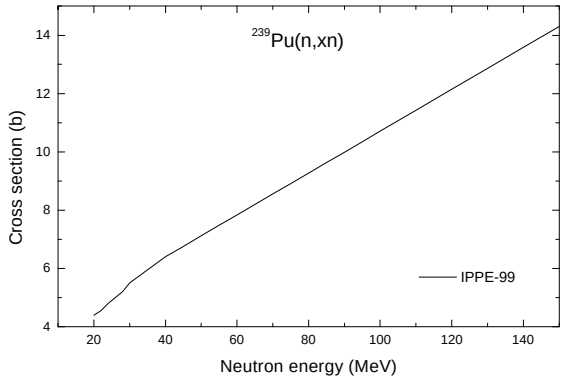

Figure 6-10. Neutron production cross section for ^{239}Pu calculated with GNASH.

6.5 CHARGED PARTICLE EMISSION CROSS SECTIONS AND SPECTRA

In order to calculate the transmission coefficients for protons, the same potential as for neutrons has been used, with the appropriate Lane components. The calculated absorption cross section for such a potential agrees rather well with Barashenkov's systematics of the proton induced reaction cross sections at high energies, but, at the present time, the experimental data are not accurate enough to test such calculations for energies close to the Coulomb barrier.

Some deficiency of the pre-equilibrium model used in the GNASH code were demonstrated in the analysis of production cross sections of deuterons and heavier charged particles [53] [61] [62]. To get more accurate evaluations of deuteron, triton and α-particle yields the modified ALICE-IPPE code was used. ALICE_IPPE describes the cluster emission on the basis of the Iwamoto-Harada model with parameters adjusted on the available experimental data of cluster yields and spectra in proton induced reactions. Deuteron emission was calculated using the quasi-direct and pick-up mechanisms. For triton emission the pick-up processes were taken into account, and for

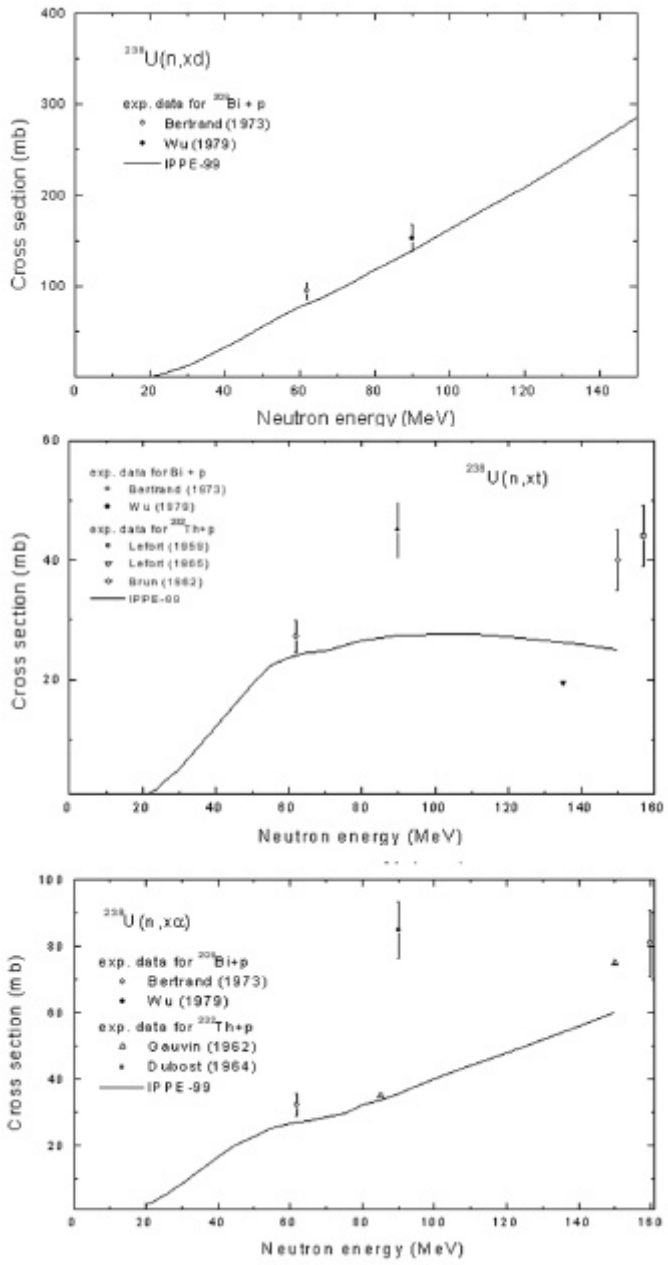

Figure 6-11.The deuteron, triton and a production cross sections for 238U evaluated on the basis of statistical calculations and experimental data.

α-particles the knock-out, pick-up and multiple pre-equilibrium emission were included into consideration.

The cross sections for the ^{238}U(n,xd), ^{238}U(n,xt) and ^{238}U(n,xα) reactions calculated in such an approach are shown in Fig. 6-11. The experimental data on the yields of the same charged particles in the proton-induced reaction on ^{209}Bi and ^{232}Th, the heaviest studied targets, are shown for the sake of comparison. Undoubtedly, uncertainties of such estimations of light cluster production cross sections are rather large, but we do not have enough experimental data to improve theoretical description essentially at the present time. On the other hand, all of these cross sections are much lower than the neutron production cross section and big uncertainties of less important cross sections seem acceptable for most applications related to the development of accelerator-driven systems.

The evaluation of the spectra and angular distributions of emitted charged particles have been done with the GNASH code, however the main parameter of the pre-equilibrium model was changed for each cluster channel to obtain the same production cross sections as with the ALICE-IPPE code.

7 SUB-CRITICAL EXPERIMENT PREPARATIONS – MUSE EXPERIMENT

7.1 INTRODUCTION

MUSE (Multiplication of an External Source) is an experimental program exploring Accelerator Driven Systems (ADS) as a radioactive waste management option. The reactor used in the experiments is called MASURCA and is situated in Cadarache in the south of France. The program started in 1995 at CEA/Cadarache in France, sponsored by EdF (Electricité de France) and Framatome. Today several research groups from different countries are participating in MUSE.
The basic idea with MUSE-experiments is to model an Accelerator-Driven System through supply a sub-critical reactor core with neutrons generated by an intense external neutron source simpler than an accelerator spallation target. In the first experiments of MUSE a strong Californium source (neutron yield of $8 \cdot 10^7\ n/s$) was placed in the centre of the core in order to sustain the neutron multiplication. In an intermediate stage, a neutron generator with (D,D and D,T)-fusion reactions is being used, while the final goal is to couple a high energetic (~GeV) proton accelerator to the rector core. Proton beam impinging a target releases a large number of neutrons in a phenomenon called spallation.

7.2 MASURCA REACTOR

MASURCA is an experimental fast neutron spectrum reactor at CEA/Cadarache. It is dedicated now to studies of accelerator driven systems in the MUSE program. The MASURCA core is rather small, the height being 60 cm and the radius ranging from 45 to 51 cm, depending on the core configurations. The reactor power is low (~5 kW) and the core cooling is provided by air.

The core of MASURCA has a very flexible design and several different core configurations are possible. The core can be loaded with different fuels (e.g. thorium, uranium and plutonium), different coolants can be used (sodium, lead, gas) and different levels of criticality are possible, both critical and sub-critical. A picture of the MASURCA-reactor seen from above is shown in Fig. 7-1. For more information about the geometry of MASURCA in the MUSE-4 experiment, see [63].

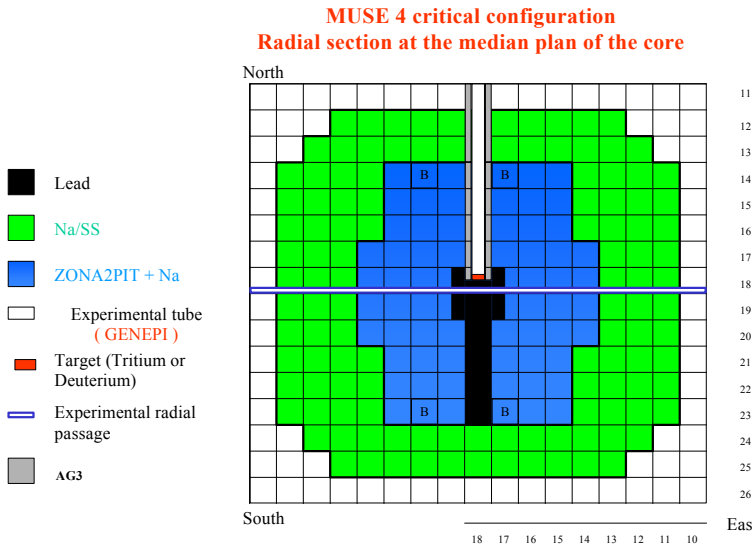

Figure 7-1. Critical configuration of MASURCA (seen from above)

The main parts of the core are:

Target: Titanium disc saturated with Tritium or Deuterium (TiD_2 or TiT_2).

Lead buffer zone: Neutrons produced in the target create a *point-like* source, which would cause a strongly peaked power distribution and a risk for overheating. To solve this problem a *buffer zone*, made of lead (or sodium), is placed around the target in order to *diffuse* the neutrons. Lead has the effect of scattering the neutrons without absorbing too much energy. Also neutron absorption is very small in lead, which results in a distributed source of neutrons with energy of about 14 MeV.

ZONA2PIT fuel cells: Every fuel subassembly (1 square in the Fig. 7-1) consists of 32 fuel rodlets and 32 sodium rodlets. The fuel is a MOX fuel (UO_2-PuO_2) enriched with 25% plutonium and the sodium rodlets are used to simulate the sodium coolant.

Na/SS shielding cells: Every shielding subassembly consists of 48 stainless steel rodlets and 16 sodium rodlets.

There is also axial and radial shielding outside the Na/SS zone, consisting of only stainless steel.

7.3 MUSE EXPERIMENTS

In order to validate experimentally the main physical principles of an accelerator driven reactor the idea is to separate the sub-critical multiplication process from the external source characteristics. This can be done by using a well-known neutron source to drive the sub-critical core. The methodology is a step-wise approach, starting from a known and tested critical reference configuration. First the characterisation of the multiplying medium alone is performed, and then insertion of an external source and investigation of the response in the medium. Different sub-critical configurations are supposed to be tested.

7.3.1 Experiments: MUSE-1 to MUSE-3

The MUSE-program started in 1995 with MUSE-1 [66]. At that time an intense Californium neutron source was used. It was placed in three different positions in the centre of the core. In MUSE-3, two years later, the Cf-source was replaced by the neutron generator SODERN/GENIE26, producing 14 MeV neutrons by (D,T)-fusion reactions. Several levels of reactivity have been investigated and MOX (UO_2-PuO_2) fuel enriched with 25% plutonium has been used. Experiments with different "buffer zones" (e.g. sodium, stainless steel and lead) have also been performed. The neutron source is surrounded by the buffer medium to simulate the diffuse properties of a spallation source. A list of all MUSE-experiments is shown below in Table 7-1.

Table 7-1: MUSE experiments in MASURCA [66][67].

Experiment	Period	Source	Fuels	Coolants	Buffers	Reactivity levels
MUSE-1	Dec **1995**	**Cf-252** $S = 8 \cdot 10^7\ n/s$	**MOX** (25% Pu)	**Sodium**	No buffer	SC = -1500 pcm
MUSE-2	July-Aug **1996**	**Cf-252** $S = 8 \cdot 10^7\ n/s$	**MOX** (25% Pu)	**Sodium**	No buffer **Sodium** **Steel**	SC_{Na} = -3400 pcm SC_{SS} = -3900 pcm
MUSE-3	Jan-April **1998**	**SODERN/ GENIE26** (d,t)-reactions	**MOX** (25% Pu)	**Sodium**	No buffer **Sodium** **Lead**	Ref = ~0 SC1 = -500 pcm SC2 = -1000 pcm SC3 = -1500 pcm SC_{Buf} = -4500 pcm
MUSE-4	April-Dec **2000** (8 months)	**GENEPI** (d,d)-reactions (d,t)-reactions	**MOX** (25% Pu)	**Sodium**	**Lead**	Ref = ~0 SC1 = -3000 pcm SC2 = -5000 pcm
MUSE-5	2001-2002? (15 months)	**GENEPI** (d,d)-reactions (d,t)-reactions	**MOX** **MOX-Th** **U (enr.)** **U-Th**	**Sodium** **Lead** **Gas**	**Lead ?**	Critical + Sub-critical
MUSE-6	2003?					

7.3.2 Planned experiments :MUSE-4, MUSE-5 …

In the MUSE-4 and MUSE-5 experiments a dedicated (D,T)-neutron generator (GENEPI) is being introduced, and other fuels, coolants and reactivity levels are also planned to be investigated [67]. The main objectives of these experiments are:

- Experimental characterisation of important neutronic properties of a multiplying sub-critical media driven by an external source. The properties can be described in terms of reactivity, external source_worth, flux and power distributions and neutron spectra etc.
- Development of sub-criticality measurements and monitoring.
- Obtaining a database to validate the predictions of the computing codes.
- Identifying possible deficiencies in the data or the methods.
- Comparing different experimental techniques for incineration of long-lived fission products.

7.3.3 Organisations participating in MUSE

There are today 11 different organisations (shown in Table 7-2) participating in MUSE.

Table 7-2: Organisations participating in MUSE

Organisation	Country	Place	Correspondent
CEA	France	Cadarache	Roland Soule
CNRS	France	Grenoble	J-M. Loiseaux
SCK/CEN	Belgium	Mol	H. Ait-Abderrahim
FZK	Germany	Karlsruhe	G. Heusener
FZJ	Germany	Juelich	P.W. Philippen
BNFL	Great Britain	Springfields	T. Abram
ENEA	Italy	Rome	M. Carta
ECN	The Netherlands	Petten	H. T. Klippel
TU DELFT	The Netherlands	Delft	J. L. Kloosterman
CIEMAT	Spain	Madrid	E. Gonzalez Romero
RIT	Sweden	Stockholm	Waclaw Gudowski

7.4 THE GENEPI ACCELERATOR

GENEPI (Generateur de Neutrons Pulsés Intenses) is a high intensity pulsed neutron generator constructed by CNRS/Grenoble and aimed at studying the physics of sub-critical reactors driven by accelerators [65] – see Fig. 7-2. A duoplasmatron providing short pulses of deuterons and a high intensity electrostatic accelerator are combined to create the 240 keV deuteron beam, leading to the tritium target in the centre of the core (0). The reaction occurring in the target is a (D,T)-fusion reaction creating high energetic (14 MeV) neutron pulses. GENEPI is in the near future going to be coupled to the MASURCA reactor in Cadarache, initiating the MUSE-4 experiment.

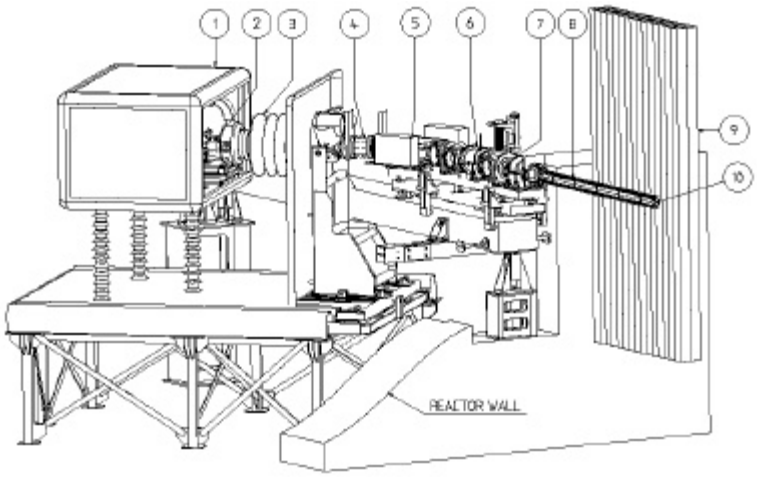

Figure 7-2. View of GENEPI. The HV terminal (1), the duoplasmatron (2), the accelerating tube (3), three electrostatic quadropoles (4,6,7), the dipole (5), the beam line (8) inside the reactor (9) towards the tritium target (19).

The specialties of GENEPI are the rather high intensity (~ 50 mA peak) combined with a pure and very short (1 μs) and sharp edged pulse – Fig. 7-3.

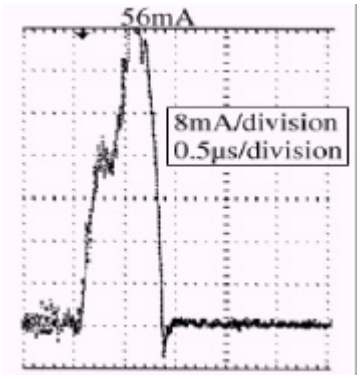

- High current – 50 mA
- Sharp and short peak – 1μs
- Frequency – 10-5000 Hz

Figure 7-3. The deuteron beam pulse.

The sharp beam pulse is desirable to be able to study the pure neutron propagation out into the fuel of the reactor, without the effect of the neutron source. Other characteristics of GENEPI are given in Table 7-3.

Table 7-3: GENEPI characteristics

Peak current	~ 50 mA
Mean current	< 200 μA
Pulse length	1 μs
Deuteron energy	240 keV
Frequency	10-5000 Hz
Beam diameter	20 mm (half max)
Target	Tritium + titanium (TiT_2)
Activity of target	12 Ci ($4.4*10^{11}$ Bq)
Neutron energy	14 MeV
Neutron production (peak)	~ $25*10^6$ n/pulse
Neutron production (mean)	~ 10^9–10^{11} n/sec

The beam is supposed to have a gaussian profile with a diameter of 20 mm at half maximum. To keep the deuterons together while they are travelling the 2-3 meters into the centre of the core, electrostatic planar electrodes are placed in the beam tube, giving a good focusing effect.

The target consists of a chemical combination of Titanium and tritium (TiD_2). A thin layer of the combination is placed on a 1.5 mm thick cylindrical (ϕ 30 mm) plate of natural copper.

7.5 MEASUREMENTS

In this section follows a brief summary of the measurements performed in the MUSE-3 experiment [64]. The neutron generator used is SODERN/GENIE26 working in both continuous and pulsed mode.

7.5.1 Static measurements and external source worth

Assume that the reactivity of the sub-critical system k_s is defined as the ratio of the fission source (S_f) and the total source (fission source + external source (generator)), as shown in 0,

$$k_s = \frac{S_f}{S_t} = \frac{S_f}{S_f + S_g} \tag{1}$$

and that k_{eff} is the reactivity of the core. Then the importance φ* of the external source (external source worth) can be defined as

$$j^* = \frac{1/k_{eff} - 1}{1/k_s - 1} = -r \cdot \frac{k_s}{1-k_s} = -r \cdot \frac{S_f}{S_g} \tag{2}$$

where

$$r = \frac{k_{eff} - 1}{k_{eff}} = 1 - \frac{1}{k_{eff}} \qquad (3)$$

In MUSE-3 measurements were performed by recording monitor counting rates, which are proportional to the power of the reactor. The measurements were repeated with the neutron generator (in continuous mode) switched OFF and ON for all configurations, and the power was recorded in each case. The external source worth φ* was also calculated. Worth to note from the measurements is that:

Switching ON the generator does not affect the neutron flux shape, but only its absolute level.

The sub-criticality level does not affect the external source worth (φ* = 1.58). This is due to the fact that the change in reactivity from one configuration to another is obtained by modifying the outer boundary of the core, and not the vicinity of the source. The relative amount of power due to the generator is therefore independent of the reactivity for these configurations.

The introduction of a sodium or a lead buffer zone decreases φ* significantly (φ* = 1.18 and 1.37 respectively). This happens because the spectrum of the neutrons produced by the source is modified by scattering reactions in the buffer (especially in the case of sodium), and they are less likely to produce fissions when they reach the core.

The external source worth seems to be approximately proportional to the power variation with the generator switched on and off.

7.5.2 Dynamic measurements

In the dynamic measurements the generator were operating in the pulsed mode, with the frequency set to 200 Hz. The results for the different configurations are shown in Fig. 7-4.

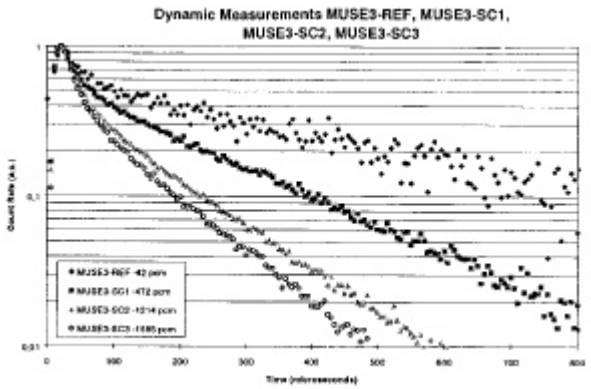

Figure 7-4. Pulsed neutron source measurements for different sub-critical levels

It is seen in Fig. 7-4 that:

- The counting rate decrease follows two exponentials. The first corresponds to instant multiplication of the neutrons injected by the generator, while the second one shows the multiplication caused by the neutrons already thermalised by the light materials in the generator.
- The counting rate drops to a nearly constant level – corresponding to the inherent source (spontaneous fission and (α,n)-reactions) – after about one millisecond.
- The more sub-critical the system is, the faster is the decay of the counting rate.

7.6 REACTOR CODES

Mainly two different codes are being used to validate the MUSE-experiments – the Monte Carlo methods MCNP [14]and MCNPX [15] and the French deterministic code ERANOS [66][68]. MCNP and MCNPX were already described in this and in the previous reports.

7.6.1 ERANOS

ERANOS is the deterministic fast reactor code developed and used by CEA. It is based on JEF2.2 cross-section data library and the codes NJOY and CALENDF are used to prepare the data.

The ERANOS code is well validated for classical sodium-cooled fast reactors and has been extended to plutonium burning cores with steel-sodium reflectors and high Pu-content. However it is not yet sufficiently validated for uranium free and nitride fuel with lead and lead-bismuth as coolants, large sub-criticalities and the presence of high-energy neutrons from spallation.

7.7 GEOMETRICAL AND PHYSICAL DATA OF MUSE-4 USED IN MCNP

7.7.1 Description of the Muse-4 geometry

An MCNP input file has three main types of cards; *cell cards*, *surface cards* and *data cards*. All surfaces needed to specify the problem geometry are listed and each is specified by the type of surface and by the location of it. The cells are constructed by the use of several surfaces enclosing a specific volume. The type of material, density, particle importance etc. are also specified in the cell cards. The data cards contain the source distribution, the tallies, the material specifications and some other options.

In this part the geometrical and physical data of the MUSE-4 experiment are accounted for. The surfaces, cells and universes described below are used in the MCNP-input file.

Figure 7-5 shows an xy-view (seen from above) of the original configuration of the MASURCA core in the MUSE-4 experiment [63].

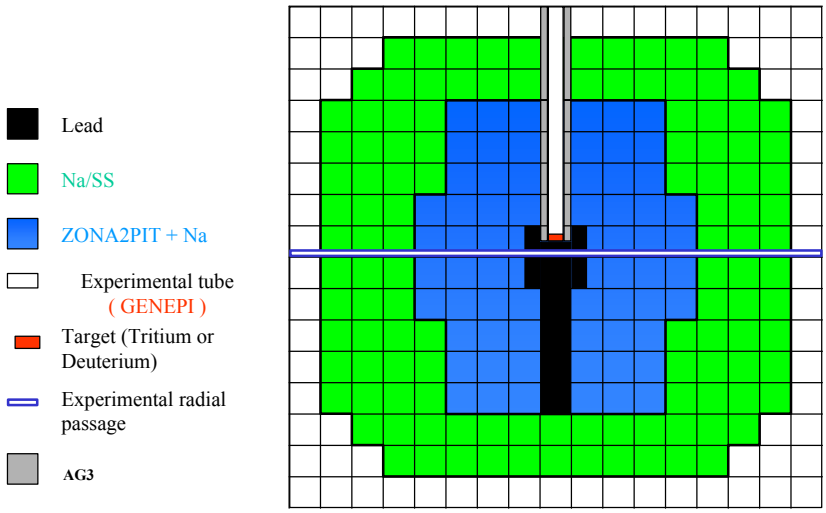

Figure 7-5. Configuration of MASURCA (xy-view) The blue area represents the fuel subassemblies, consisting of 32 fuel rodlets and 32 Na rodlets (coolant). The green area shows the Na/SS shielding subassemblies, consisting of 16 Na rodlets and 48 stainless steel rodlets.

Figure 7-6 shows a yz- and an xz-view of the core.

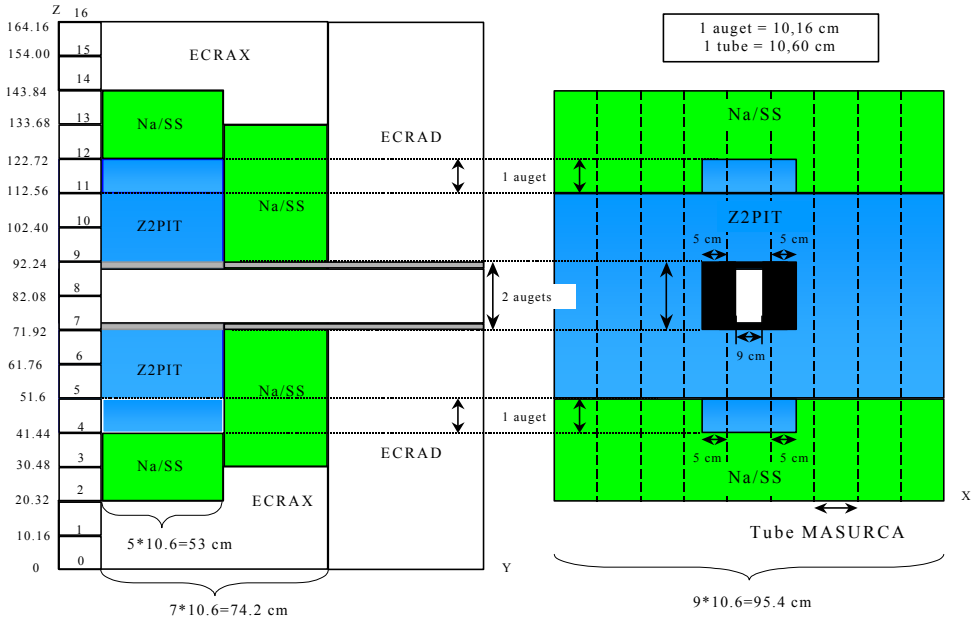

Figure 7-6. Configuration of MASURCA (yz- and xz-view)

7.7.2 MCNP input: universes and the smallest units

Universe in the MCNP input is a way to describe geometry of a simulated system. Universe is either a lattice or an arbitrary collection of cells, which are then filling other

cells. In the description of the Muse-4 geometry in the MCNP-input file two levels of universes are used. The rodlet is the smallest unit of the reactor and is shown with its location in Figure 7-7. The surface numbers are printed in blue and the cell numbers in red.

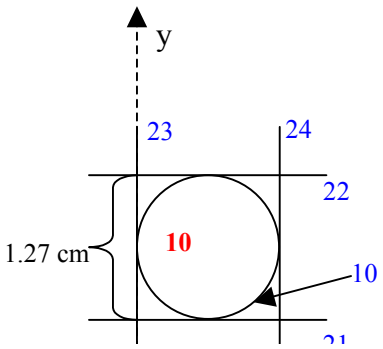

Figure 7-7. The Rodlet – Smallest unit

Surfaces definitions
21 py 0.22
22 py 1.49
23 px 0
24 px 1.27

The next level of universes contains the subassemblies – Fig. 7-8, which are filled with the rodlets.

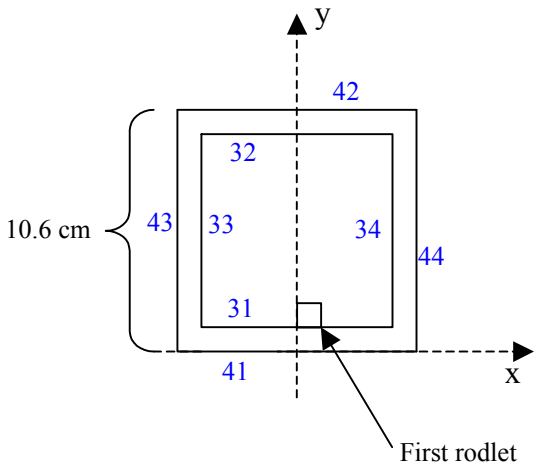

Figure 7-8. The inner surfaces limit the rodlet universes (auget) and the outer are the limits of the subassembly (tube).

Surfaces definitions	
31 py 0.22	41 py 0
32 py 10.38	42 py 10.6
33 px -5.08	43 px -5.3
34 px 5.08	44 px 5.3

This universe finally fills different parts of the reactor.

7.7.3 Z2PIT Fuel Zone (Blue inner area)

The Z2PIT fuel subassemblies (shown in Fig. 7-8) are filled with 32 fuel rodlets ($UPuO_2$) and 32 Na rodlets, according to Fig. 7-9.

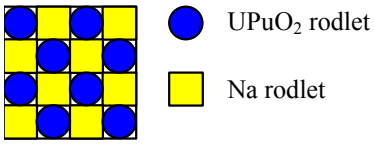

Figure7- 9. Z2PIT basic cell. One subassembly consists of 4 of these basic cells.

The dimensions and the surfaces enclosing the whole Z2PIT fuel zone are shown in Figs 7-10 and 7-11.

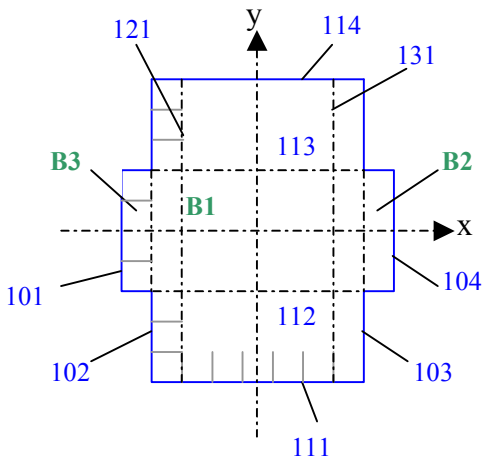

Surfaces definitions	
101 px -47.7	111 py -53
102 px -37.1	112 py -21.2
103 px 37.1	113 py 21.2
104 px 47.7	114 py 53

Figure 7-10. xy-view of the Z2PIT Fuel Zone. B1 to B3 are subzones for practical reasons in the MCNP-input .

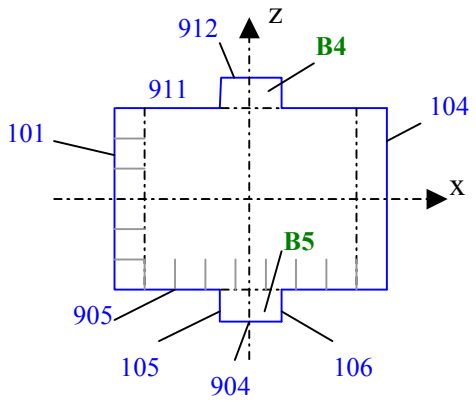

Surface definitions	
105 px –10.3	904 pz 41.44 (lev 4)
106 px 10.3	905 pz 51.60 (lev 5)
	911 pz 112.56 (lev 11)
	912 pz 122.72 (lev 12)

Figure 7-11. xz-view of the Z2PIT Fuel Zone

7.7.4 Na/SS Zone (green area)

The Na/SS shielding subassemblies are filled with 16 Na rodlets and 48 stainless steel rodlets, according to Fig. 12.

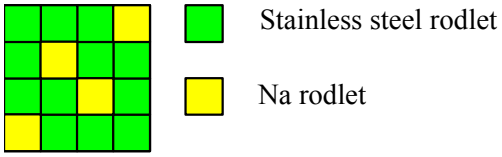

Figure 7-12. Na/SS basic cell. One subassembly consists of 4 of these basic cells.

The dimensions and the surfaces enclosing the whole Na/SS shielding zone are shown in Fig. 7-13.

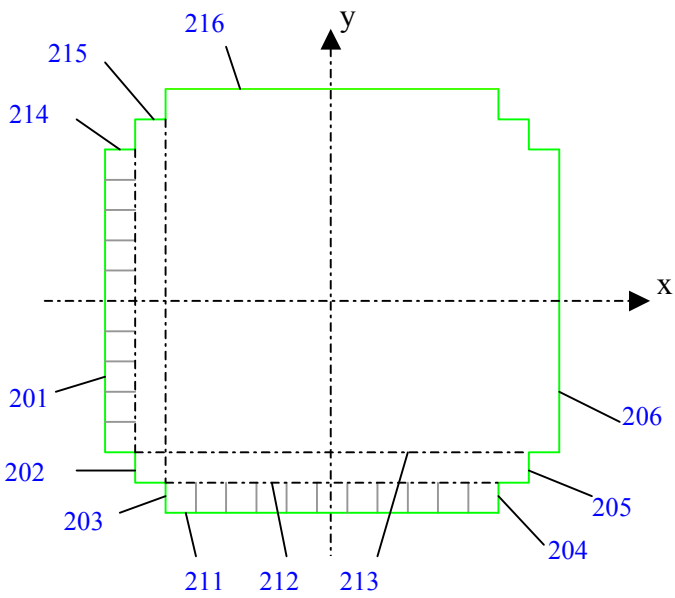

Surface definitions	
201 px -79.5	211 py -74.2
202 px -68.9	212 py -63.6
203 px -58.3	213 py -53
204 px 58.3	214 py 53
205 px 68.9	215 py 63.6
206 px 79.5	216 py 74.2

Figure 13. xy-view of the Na/SS Zone

7.8 MATERIAL COMPOSITION

The composition of the heavy isotopes (uranium to americium) in the fuel rodlets is also listed in Table 7-4.

Table 7-4: Composition of heavy isotopes in the fuel rodlets

	Fraction of element	**Fraction of heavy isotopes**	**Fraction of total fuel**
S Uranium		**72.5 %**	**21.8 %**
U-235	0.3 %	0.24 %	
U-238	99.7 %	72.3 %	
S Plutonium		**27.1 %**	**8.2 %**
Pu-239	77.5 %	21.0%	
Pu-240	18.9 %	5.1 %	
Pu-241	1.4 % (3.1 %)	0.39 % (0.85%)	
Pu-242	0.7 %	0.18%	
S Americium		**0.67 % (0.22 %)**	**0.21 % (0.07 %)**
Am-241	100 %	0.67 % (0.22 %)	

7.9 MCNP CALCULATIONS OF DIFFERENT CONFIGURATIONS OF MUSE-4

In this part, calculations of several different configurations of the MASURCA core, performed with MCNP, are accounted for. All configurations are shown in Figs 7-14 – 7-16. and the results are given in Table 7-5.

However, it is important to observe that all calculations have been based on the fresh fuel composition, dated to April 1:st 1984. All results, except the values coloured with blue and labelled as “corrected values of k-eff”, therefore contain a systematic error, due to the decay of Pu-241 to Am-241.

7.10 RUNNING MCNP

The cross section data library primarily used is JEF2.2. For some isotopes there exist no cross section data and in these cases the amount of the isotope is added to the isotope with the same parity (odd to odd or even to even) next to it. If the amount of the isotope is very small it has in some cases been excluded.

As a first attempt a criticality calculation has been made with the source card KCODE. 1000 neutrons were simulated each cycle and 100 effective cycles were run.

7.10.1 Subcritical core calculations - CEA configurations

Recent calculations performed by several members of the MUSE-consortium have shown that the loading configurations initially proposed by CEA have given too high values of k-eff. Therefore CEA has changed the configurations in order to achieve three

levels of reactivity, 1.00, 0.97 and 0.95. The modifications only apply to the radial loadings, and the axial configurations are identical to those previously proposed. The values obtained at RIT with MCNP-calculations for these calculations are shown in Table 5 and the new configurations are shown in the figures below.

Table 7-5: k-eff values for different configurations of the CEA proposal. The calculations are based on the composition of the fresh fuel, dated to 1984 with corrected values in blue

	k-eff fresh fuel	Standard deviation	Expected k-eff	Reactivity	Difference to Ref	# Sub.ass.	# Cells	Corrected values of k-eff
CEA-orig.	1.06587	195 pcm		+6587 pcm	-	78	1248	**1.04939**
CEA-Ref	1.03223	203 pcm	1.00	+3223 pcm	0	67	1072	**1.01851**
CEA-SC1	1.00123	206 pcm	0.97	+123 pcm	-3100 pcm	58	928	**0.98329**
CEA-SC2	0.98495	177 pcm	0.95	-1505 pcm	-4728 pcm	55	880	**0.96546**

CEA reference level

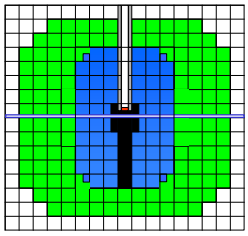

k-eff =1.03223, std = 203 pcm (fresh fuel, dated to 1984)

Figure 7-14. Reference level(Ref) proposed by CEA (67 subassemblies)

CEA - SC1

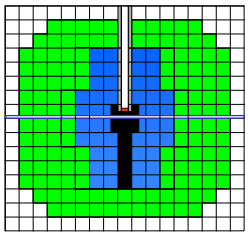

k-eff =1.00123, std = 206 pcm (fresh fuel, dated to 1984)

Difference to Ref = -3100 pcm

Figure 7-15. First sub-critical state (SC1) proposed by CEA (58 subassemblies)

CEA - SC2

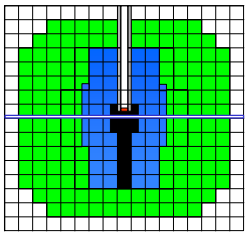

K-eff =0.98495, std = 177 pcm (fresh fuel, dated to 1984)

Difference to Ref = -4728 pcm

Figure 7-16. Second sub-critical state (SC2) proposed by CEA (55 subassemblies)

7.11 RESULTS AND CONCLUSIONS

7.11.1 Correction of fuel composition

All calculations accounted for in the previous sections were based on the composition of the fresh fuel, dated to April 1:st 1984 [63], which has caused a consequent error in the results. Plutonium-241, which at first constituted 0.85 % of the heavy nuclides in the fuel (Table 7-4), β-decays to Americium-241 with a half-life of 14.35 years. Almost 16 years have passed since the composition was specified, which means that a little more than 50 % of the Pu-241 today has been converted to Am-241. Am-241 has a much lower fission cross-section than Pu-241 and this decay of Pu-241 therefore decreases the reactivity. Hence the results obtained with the composition from 1984 are too high. The correction of the fuel composition should be made according to the following two relationships.

$$N_{Pu-241} = N_{0\,Pu-241} e^{-\ln 2 \cdot 16 / 14.35} = 0.4617 \cdot N_{0\,Pu-241} \qquad (1)$$

$$N_{Am-241} = N_{0\,Am-241} + \left(1 - N_{Pu-241}\right) = N_{0\,Am-241} + 0.5383 \cdot N_{0\,Pu-241} \qquad (2)$$

The amount of Pu-241 and Am-241 before and after the correction is shown in Table 7-6.

Table 7-6: Amount of Pu-241 and Am-241 before and after correction for the β-decay

Nuclide	April 1:st 1984 (Before correction)		April 1:st 2000 (After correction)	
	Atom density [n/cm*barn]	Fraction of heavy nuclides	Atom density [n/cm*barn]	Fraction of heavy nuclides
Pu-241	1.70599E-04	0.85 %	7.87656E-05	0.39 %
Am-241	4.53162E-05	0.22 %	1.37150E-04	0.67 %

7.11.2 Conclusions

The results obtained for the configurations proposed by Figs 7-14 – 7-16, with the corrected fuel composition, are shown in Table 7-7.

Table 7-7: Values of k-eff for the configurations proposed by CEA. Corrected composition of the fuel.

	k-eff	Standard deviation	Expected k-eff	Reactivity	Difference to Ref	# Sub.ass.	# Fuel cells
CEA-orig.	1.04939	205 pcm		+4939 pcm	-	78	1248
CEA-Ref (0)	1.01851	188 pcm	1.00	+1851 pcm	0	67	1072
CEA-SC1 (0)	0.98329	182 pcm	0.97	-1671 pcm	-3522 pcm	58	928
CEA-SC2 (0)	0.96546	194 pcm	0.95	-3454 pcm	-5305 pcm	55	880

The values of k-eff are, despite the correction for the β-decay of Pu-241, still higher than the values expected by CEA. The difference is about 1500 pcm. This inaccuracy, probably due to differences in data libraries, needs to be further investigated and compared with the calculations performed by the other participants of the MUSE-4 consortium.

8 SPALLATION TARGET DEVELOPMENT

The International Science and Technology Centre Project # 559 "Pilot flow lead-bismuth target of 1 MWth for accelerator-based systems" is a collaborative project between Institute of Physics and Power Engineering (IPPE) in Obninsk, Los Alamos National Laboratory (LANL), Royal Institute of Technology and CEA-Cadarache. Funding parties of this project are USA, EU and Sweden.

The purpose of the project is to develop a heavy metal-Pb/Bi eutectic- flow target, which possesses the best features for producing neutrons at a high power proton accelerator. Thus, the technical key problems of a flowing Lead-Bismuth 20 MW-power target should be investigated. Such a technical base will be established by the design of a pilot lead-bismuth 1 MW power target. It is decided that the pilot target will be tested at the LANSCE accelerator at LANL (LANSCE: 800 MeV, 1.5 mA linear proton accelerator) after extensive off-beam tests, first in Obninsk year 2000 and then in Los Alamos.

The spallation target has been already manufactured, and is being now assembled together. Fig. 8-1 shows the main components of the target and corresponding manufactured pieces. Fig. 8-2 shows the photography of the target body. Fig. 8-3 presents one of the most critical part of the target – a target window with important pieces of its fastening. Fig. 8-4 shows a diffuser plate, being placed just behind the target window to ensure homogeneous coolant flow and efficient cooling of the hottest volume of the target.

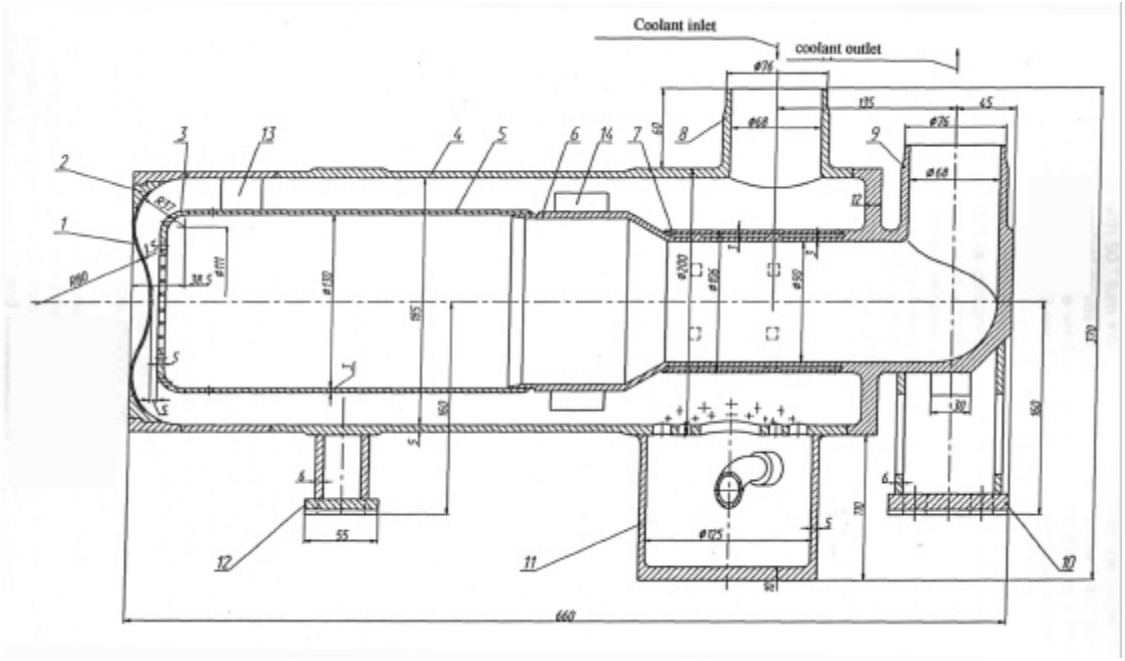

Figure 8-1. The spallation target. Main components of the target: 1 - window, 2 - window support, 3 - diffuser plate (see Fig. 8-3), 4 - target hull (see Fig. 8-2), 5 - inner channel.

Figure 8-2. Components of the spallation target body.

Figure 8-3. The spallation target window with some constructional components.

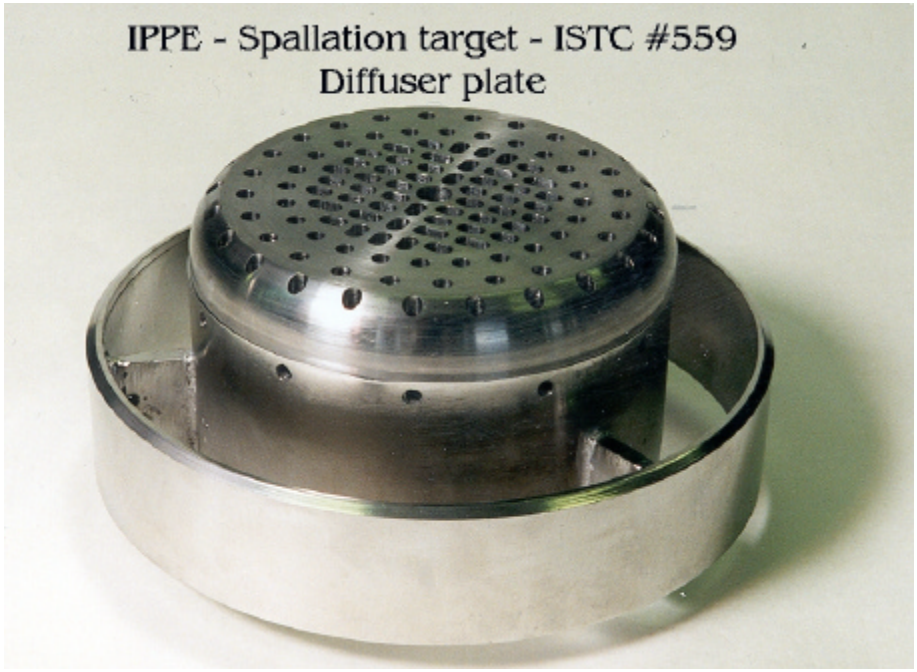

Figure 8-4. A diffuser plate.

9 SEMINARS, CONFERENCES AND INTERNATIONAL INTERACTION

PANIC 99 – Particles and Nuclei Int. Conference, Uppsala May 1999: W. Gudowski, "Transmutation of Nuclear Waste", Nuclear Physics A663&664 (2000) 169c-182c (invited talk)

ADTTA-99 – 3rd International Conference on Accelerator Driven Technologies and Applications, Prague, June 7-11, 1999

Presented papers:

V. Barashenkov, W, Gudowski, A. Polanski, "Integral high-energy nucleon-nucleus cross-sections for mathematical experiments with electronuclear facilities", In Proc. of ADTTA-99 – 3rd International Conference on Accelerator Driven Technologies and Applications, Prague, June 7-11, 1999

J. Cetnar, W. Gudowski and J. Wallenius, "Transmutation calculations with Monte-Carlo continuous energy burnup system (MCB) – IAEA ADS-benchmarks, In Proc. 3rd. International Conference on Accelerator Driven Technologies and Applications, Prague, June 7-11, 1999.

A.V. Ignatyuk, V. Lunev, Yu. Shubin, E. Gai, N. Titarenko and W. Gudowski, "Neutron cross section evaluation for ^{232}Th up to 150 MeV", In Proc. 3rd. International Conference on Accelerator Driven Technologies and Applications, Prague, June 7-11, 1999

J. Wallenius, K. Tucek, W. Gudowski and C. Sanders, "Neutronics of a sub-critical system burning unrecycled LWR waste. ", In Proc. 3rd. Int. Conf. on Accelerator Driven Transmutation Technologies, Prague, June 7-11, 1999. (oral presentation of J. Wallenius)

J. Wallenius, K. Tucek, W. Gudowski and C. Sanders, "Burnup in sub-critical system with flat power density. ", In Proc. 3rd. Int. Conf. on Accelerator Driven Transmutation Technologies, Prague, June 7-11, 1999.

W. Gudowski, "Overview of national ADS-projects" (invited).

Accelerator Transmutation of Waste –World Expert Meeting, DOE, Washington, DC, 15-16 March 1999 and 15-16 July 1999

Waclaw Gudowski (invited speaker and expert), "Status of ATW technology and research needs from the Swedish perspective and opportunities for international collaboration", In Proceedings of Workshop: Accelerator Transmutation of Waste – World Expert Meeting, DOE, Washington, DC, 15-16 March 1999.

Accelerator Transmutation of Waste – Second World Expert Meeting, DOE, Washington, DC, 15-16 July 1999

NATO Advanced Research Workshop "Techniques and Selected Applications of Nuclear Physics", Krzyze, Poland, September 2-4, 1999:

W. Gudowski, "Transmutation of Isotopes Ecological and Energy Production Aspects", Acta Physica Polonica B, Vol. 31 (2000)

NEA/OECD Expert Group for "Comparative Study of ADS and FR in Advanced Nuclear Fuel Cycles", meetings in Paris May 10-11 and October 25-26, 1999. Participation: Waclaw Gudowski

IAEA Advisory Group Meeting on ADS Programmes: "Review of National Accelerator Driven Systems (ADS) Programmes"- Taejon, Republic of Korea, 1-4 November 1999. Participation: Waclaw Gudowski

IAEA Consultancies on "Proposals for New Co-ordinated Research Projects (CRPs) on Accelerator Driven Systems (ADS)", "Non-Conventional Nuclear Energy Systems" and elopment for ADS R&D". 29 November to 8 December 1999.Participation: Waclaw Gudowski

NEA/OECD Workshop on Utilisation and Reliability of High Power Accelerators, Aix-en-Provence, France, 22-24 November 1999. Participation: Waclaw Gudowski

R.J.M. Konings, H. Boussier, H. Gruppelaar. W. Gudowski, J.P. Meulders, S. Pilate, C.Rubbia, "Transmutation: the state of the art after the Fourth Framework **EURADWASTE Conference, Luxemburg**, 1999.

Visit to the department of **Material Physics of Liverpool University**. Lecture on "An introduction to accelerator driven transmutation of nuclear waste". Janne Wallenius - February 1999.

International Conference on Future Nuclear Systems, GLOBAL 99, in Jackson Hole, September 1999. Participation: Janne Wallenius.

REFERENCES

[1] S.L. Beaman, “Actinide recycle in LMFBRs as a waste management alternative”, First international conference on nuclear waste transmutation, page 61, University of Texas, 1980

[2] A.Languille et al., “CAPRA core studies - the oxide reference option”, International Conference on Future nuclear systems, GLOBAL 95, page 874, ANS 1995

[3] T. Mukaiyama, “Importance of the double strata fuel cycle for minor actinide transmutation”, Third international information exchange meeting, page 30, OECD/NEA, 1994

[4] H. Murata and T. Mukaiyama, “Fission reactor studies in view of reactor waste -Kerntechnik, 45, page 23, 1984

[5] C. Rubbia et al., “A realistic plutonium elimination scheme with fast energy amplifiers and Thorium-Plutonium fuel”, CERN, AT/95-53 (ET) 1995

[6] M. Salvatores et al., Nuclear Instruments and Methods A, 414, page 5, 1997

[7] In High level Radioactive Waste management alternatives, BNWL-1900, Batelle Northwest 1974

[8] T. Takizuka et al. Conceptual design of transmutation plant. In Proc. Specialist meeting on accelerator driven transmutation technology, page 707, Saltsjöbaden 1991

[9] M. Takano et al., ”Synthesis of americium mononitride by carbothermic reduction method”, International Conference on Future nuclear systems, GLOBAL 99, ANS, 1999

[10] T. Wakabayashi et al., “Status of study on TRU transmutation in LFMBRs”, Transactions of American Nuclear Society 64, page 556, 1991

[11] J. Wallenius et al., “Application of burnable absorbers in accelerator driven systems”, submitted to Nuclear Science and Engineering

[12] P. Wydler, OECD/NEA Benchmark on minor actinide transmutation in accelerator driven systems. OECD/NEA 1999.

[13] H.S. Khalil and R.N. Hill, Evaluation of Liquid Metal Reactor Design Options for Reduction of Sodium Void Worth. Nuclear Science and Engineering 109, page 221 (1991)

[14] Briesmeister, J., MCNP^{TM} - A general Monte Carlo N-Particle Transport Code Version 4B LA-12625-M, Los Alamos National Laboratory, 1997.

[15] H.G. Hughes, K.J. Adams, M.B. Chadwick, J.C. Comly, S.C. Frankle, J.S. Hendricks, R.C. Little, R.E. Prael, L.S. Waters, and P.G. Young, Jr., Status of the MCNP^{TM} / LCS^{TM} Merger Project, Proceedings of the Radiation Protection and Shielding Topical Conference, Nashville, Tennessee, April 19-23, 1998.

[16] Richard B. Firestone, Virginia S. Shirley, Coral M. Baglin, S.Y. Frank Chu, and Jean Zipkin, “The 8th edition of the Table of Isotopes, book and CD-ROM”,. John Wiley & Sons, Inc., 1996.

[17] EURATOM 1996. Laying Down Basic Safety Standards for the Protection of the Health of Workers and the General Public from the Dangers Arising from

Ionizing Radiation. Council Directive 96/29 Euratom of May 13, 1996. Official Journal of the European Communities, Vol. 39, No. L 159, June 29, 1996.

[18] M.J. Bell, ORIGEN- The ORNL Isotope Generation and Depletion Code, ORNL-4628 UC-32, 1973

[19] F. M. Mann and R. E. Schenter, Nucl. Sci. Eng. 63 (1977)

[20] A. Wahl, Phys. Rev. C 32 184 (1985)

[21] M. L. Woosley, R. A. Rydin, "Dynamic Analysis of an Accelerator-Driven Fluid-Fueled Subcritical Radioactive Waste Burning System, Nuclear Science and Engineering, 129, 15-50, 1998.

[22] R. A. Rydin, M. L. Woosley, "Evidence of Source Dominance in the Dynamic Behavior of Accelerator-Driven Systems", Nuclear Science and Engineering, 126, 341-344, 1997.

[23] T. D. Burns, R. A. Rydin, P. Ravetto, "Perturbation Theory and Kinetics of Subcritical Accelerator-Driven Systems", 3rd International Conference on Accelerator Driven Transmutation Technologies and Applications, Praha, June 3-7, 1999.

[24] T. D. Burns, R. A. Rydin, "Dynamic Analysis of Source Driven Sub-critical Nuclear Systems", International Conference on the Physics of Nuclear Science and Technology, New York, October 5-8, 1998.

[25] A.D'Angelo, G. Bianchini, M. Carta, "Preliminary Analysis of Neutronic-Source Transients in a small ADS Prototype", 3rd International Conference on Accelerator Driven Transmutation Technologies and Applications, Praha, June 3-7, 1999.

[26] F. E. Dunn, D. C. Wade, "Estimates of Thermal Fatigue due to Beam Interruptions for an ALMR-type ATW", 2nd Workshop on Utilization and Reliability of High Power Proton Accelerators, Aix-en-Provence, November 22-24, 1999.

[27] J. F. Jackson, W. E. Kastenberg, "Space-Time Effects in Fast Reactor Dynamics", Nuclear Science and Engineering, 42, 278-294, 1970.

[28] Buono, S., and Rubbia, C., 1996, Simulation of a Total Loss of Power accident in the Energy Amplifier, CERN/ET Internal note 96-015.

[29] Cheng, X., Erbacher, F.J., Neitzel, H.J., 1997, Convection and radiation heat transfer in a passive containment cooling system, Proc. ICONE-5 Conf.

[30] Carluec B., 1999, Framatome, personal communication to H.Wider

[31] Cinotti, L., and Corsini, G., A proposal for enhancing the primary coolant circulation in an ADS, unpublished

[32] Computational Dynamics Ltd., 1999, *Methodology Volume 3.10*

[33] Delcorio, B., Choi, K-J., Oct.-Dec. 1991, Analysis of Direct Liquid-Solid Contact Heat Transfer in Monodispersed Spray Cooling, J. of Thermophysics, Vol. 5, No. 4

[34] Eckert, E.R.G., Drake, R.M., 1959, *Heat and Mass Transfer*, McGraw-Hill Book Company Inc., New York

[35] Fox, W.F., McDonald, A.T., 1978, *Introduction to Fluid Mechanics*, John Wiley & Sons, New York, ISBN 0-471-01909-7, pp. 63

[36] Hunsbedt, A., Magee, P.M., Design and performance of the PRISM natural convection decay heat removal system, Proc. Int. Topical Meeting on Safety of Next Generation Power Reactors, p.844-851, 1988

[37] Incropera, F.P., DeWitt, D.P., 1996, *Fundamentals of Heat and Mass Transfer,* ISBN 0-471-30460-3, Johan Wiley & Sons, New York, pp. 657

[38] Krieg, 1999, private communication to Wider H.

[39] Novikova, N., Pashkin, Y., Chekunov, V., 1999, *Some features of subcritical blankets cooled with lead-bismuth,* Proc. 3rd Int. Conf. Accelerator-Driven Transmutation Technologies and Applications, ADTTA 99

[40] Pershagen, B., 1989, *Light Water Reactor Safety,* Pergamon Press, Oxford, England, ISBN 0-08-035915-9, pp. 131

[41] Rousanov, A.E., et al. 1998, *Design and study of cladding steels for fuel elements of NPP using heavy coolant,* Proc. Heavy Liquid Metal Coolants in Nuclear Technology, HLMC 98. IPPE

[42] Van Tuyle, G.J., Slovik, G.C., Chan, B.C., Kennett, R.J., Cheng, H.S., and Kroeger, P.G., Summary of Advanced LMR Evaluations – PRISM and SAFR, Brookhaven National Laboratory, Oct. 1989, p.87-91.

[43] W. Gudowski, Co-ordinator, "Impact of Accelerator Based Technologies on Nuclear Fission Safety - IABAT-project. Final report", Contract no: FI4I-CT96-0012, 2000 (in print)

[44] Proceedings of the NEA Specialist Meeting on Intermediate Energy Nuclear Data: Models and Codes, May 30-June 1 1994, Issy-les-Moulineaux, France.

[45] M.B. Chadwick et al., New high-energy evaluated nuclear data libraries for the accelerator production of tritium program, 9th Nuclear explosives code developer's conference, Oct. 21-25 (1996), San Diego.

[46] A.J. Koning, Requirements for an Evaluated Nuclear Data File for Accelerator-Based Transmutation, NEA Data Bank Report NEA/NSC/DOC (93) 6.

[47] P.F. Rose and C.L. Dunford (eds.), Data formats and procedures for the evaluated nuclear data file ENDF-6, Brookhaven National Laboratory report BNL-NCS-44945, 1990.

[48] G.N. Manturov, V.P. Lunev, L.V. Gorbachova, VANT, Yadernye Constanty, 1983, v.1 (50), p.50.

[49] J. Raynal, Mater. Of Workshop on Nuclear Model Computer Codes. 16 Jan - 3 Feb. 1984, Trieste.

[50] P.G. Young et al., Comprehensive nuclear model calculations: Introduction to the theory and use of the GNASH code, Workshop on Nuclear Reaction Data and Nuclear Reactors, April 15 - May 17 1996, Trieste, Italy.

[51] A.V. Ignatyuk. Reference Input Parameter Library for Nuclear Model Calculations - Handbook. IAEA - TECDOC, Vienna, 1998, ch. 5.

[52] H. Vonach, A. Pavlik, M.B. Chadwick, R.C. Haight, R.O. Nelson, S.A. Wender, and P.G. Young, "207, 208Pb(n,xn) Reactions for Neutron Energies from 3 to 200 MeV," Phys. Rev. C50, 1952 (1994)

[53] M.B.Chadwick, P.G. Young, "GNASH Calculations of the Neutron and Proton Induced Reactions for Lead Isotopes and Benchmarking of Results," Report T-2-96, Los Alamos National Laboratory (1996)

[54] V. Barashenkov, Cross Sections of Particle and Nucleus Interactions with Nuclei (Russian), JINR, Dubna, 1993.

[55] V.M. Pankratov, “Fission Cross Sections of Th-232, U-233, U-235, Np-237, U-238 for 5-37 MeV Neutrons,” Atomnaya Energia, 14, 177 (1963)

[56] R.K. Smith, R.K. Henkel, R.A. Noble, BAP 2,(1957)

[57] A.V. Ignatyuk, G.A. Kudyaev, A.R. Junghans, M. de Jong, M.G. Clerc, and K.H. Schmidt, “Analysis of dissipation effects in nuclear fission observed in the fragmentation of 238U projectiles,” Nucl. Phys. A593, 519 (1995)

[58] J. Fréhaut, “Nu-bar Results at Bruyères-le-Châtel”, Private communication to EXFOR-21685 (1976).

[59] Yu.A. Korovin, A.Yu. Konobeev, V.P. Lunev, P.E. Pereslavtsev, A.Yu. Stankovski, “Evaluated Data File for U-238,” Obninsk, Institute of Nuclear Power Engineering (1996)

[60] C. Kalbach, F.M. Mann, “Phenomenology of Continuum Angular Distributions. I. Syste-matics and Parameterization,” Phys. Rev. C23, 112 (1981)

[61] A. Iwamoto, K. Harada, “Mechanism of Cluster Emission in Nucleon-Induced Preequilibrium Reactions,” Phys. Rev. C26, 1821 (1982)

[62] A.I. Dityuk, A.Yu. Konobeyev, V.P. Lunev, Yu.N.Shubin. “New Advanced Version of Computer Code ALICE-IPPE,” Report INDC(CCP)-410, IAEA, Vienna (1998)

[63] W. Assal, C.A. Bompas and R. Soule, "Geometrical and physical data for the MUSE 4 experiment", CEA/Cadarache (1999).

[64] J.F. Lebrat, “Experimental investigation of multiplying sub-critical media in presence of an external source operating in pulsed or continuous mode: The MUSE-3 experiment”, CEA/Cadarache.

[65] J.M De Conto, on behalf of the GENEPI team, “GENEPI: A high intensity deuteron accelerator for pulsed neutron production”, CNRS/Grenoble

[66] R. Jacqmin, “Accelerator-Based Neutron Sources and Experiments”, Lecture at FJSS’98, Cadarache (1998)

[67] R. Soule, “Proposal for the 5th R&D Framework Program”, CEA/Cadarache (1999)

[68] “The neutronic formulaire for fast neutron reactors”, CEA

[69] F. H. Attix, W. C. Rowsch, E. Tochilin “Radiation Dosimetry”, Academic Press (1969)